Catalysis Science & Technology

Homogeneous Oxidation of C–H bonds with m-CPBA Catalysed by a Co/Fe System: Mechanistic Insights from the Point of View of the Oxidant

Journal:	*Catalysis Science & Technology*
Manuscript ID	CY-ART-11-2021-001991
Article Type:	Paper
Date Submitted by the Author:	02-Nov-2021
Complete List of Authors:	Nesterova, Oksana; Instituto Superior Técnico, Universidade de Lisboa, Centro de Química Estrutural Kuznetsov, Maxim; Instituto Superior Tecnico, Centro de Quimica Estrutural Pombeiro, Armando; Universidade de Lisboa, Centro de Química Estrutural, Instituto Superior Técnico Shul'pin, Georgiy; Semenov Institute of Chemical Physics, Nesterov, Dmytro; Universidade de Lisboa Instituto Superior Técnico,

ARTICLE

Homogeneous Oxidation of C–H bonds with *m*-CPBA Catalysed by a Co/Fe System: Mechanistic Insights from the Point of View of the Oxidant

Received 00th January 20xx,
Accepted 00th January 20xx

DOI: 10.1039/x0xx00000x

Oksana V. Nesterova,[a] Maxim L. Kuznetsov,[a] Armando J. L. Pombeiro,[a,b] Georgiy B. Shul'pin[c,d] and Dmytro S. Nesterov*[a]

Oxidations of C–H bonds with *m*-chloroperoxybenzoic acid (*m*-CPBA) catalyzed by transition metal complexes are known to proceed through a number of routes, from the non-selective free radical to selective concerted and metal-mediated ones. However, there is lack of understanding of the *m*-CPBA oxidative behavior, reaction mechanisms and factors that trigger its activity. An experimental and theoretical investigation of sp^3 C–H bonds oxidation with *m*-CPBA in the presence of the pre-catalyst $[Co^{III}_4Fe^{III}_2O(Sae)_8]\cdot 4DMF\cdot H_2O$ (**1**) (H_2Sae = salicylidene-2-ethanolamine) and HNO_3 promoter has been performed herein. The catalytic system **1**/HNO_3/*m*-CPBA allows mild hydroxylation of tertiary C–H bonds with 99% retention of stereoconfiguration of model alkane substrates, supported by high TOFs up to 2 s^{-1} (for *cis*-1,2-dimethylcyclohexane) and TONs up to 1.4×10^4 (at 50 °C). The catalytic effect of **1** is seen at *ppm* level, while 1000 *ppm* (0.1 mol%) loading allows 1000-fold increase of the initial reaction rate up to 9×10^{-5} M s^{-1}. The reaction mechanism was investigated by means of combined kinetic studies (including isotope effects), isotopic labeling ($^{18}O_2$, $H_2{}^{18}O$, D_2O), ESI-MS spectroscopy and DFT theoretical studies. The results suggest that the main oxidation pathway proceeds through a concerted mechanism involving a cobalt-peroxo C–H attacking species or via a cobalt-oxyl species (rebound process), rather than a free-radical pathway. Remarkably, the Co(III) catalyst does not change its oxidation state during the most energetically favored pathway, consistent with a metal-ligand cooperativity. The chlorobenzene radical is responsible for H abstraction in the non-selective side route, which is efficiently suppressed by the acidic promoter. Finally, signs for slow direct oxygen exchange between *m*-CPBA and water in the presence of a proton or a metal complex are found, suggesting that the results of ^{18}O-tests should be treated cautiously when *m*-CPBA is used as the oxidant.

Introduction

Selective catalytic oxidation of sp^3 C–H bonds remains a challenge in contemporary chemistry.[1-8] The high energy of the C–H bond and the saturated character of alkanes[9] foresee the use of strong terminal oxidants, such as dioxygen or various peroxides (hydrogen peroxide or alkyl hydroperoxides, peracids, etc). Peroxides, being readily available oxidants for preparative chemistry, are highly prone to low-selective free radical activity,[10, 11] while the activation of dioxygen by metal complexes is an uncommon task.[12] Complexes of iron or manganese can constitute catalysts for selective oxidation of alkanes (as well as alkenes and other substrates) with hydrogen peroxide as a terminal oxidant.[4, 13] The origin of selectivity in these systems concerns high-valent metal-oxo (HVMO) species,[14-16] stabilized by sophisticated capping or macrocyclic N-donor ligands which require laborious syntheses, thus hampering an overall potential impact.[4, 17] Catalytic activity of heterometallic complexes in C–H oxidation,[18] particularly involving those metals forming HVMO species, is of special interest due to the recognized synergic effect of few dissimilar metals.[10, 19-21]

Peroxides constitute a large class of oxidants, where one compound, *m*-chloroperbenzoic acid (*m*-CPBA), stands apart from the other members of this family due to its unusually complex oxidative behaviour that combines a range of pathways − from a free radical to concerted ones. In modern organic chemistry, *m*-CPBA is an inexpensive, stable, organic-soluble, versatile oxidation reagent, routinely used in Baeyer–Villiger oxidation of ketones, selective epoxidation of olefins and other valuable processes.[22] It was reported that *m*-CPBA, taken in large excess, is able to oxidize alkanes under catalyst-free conditions, showing some limited stereoselectivity.[23-25] Furthermore, the large amounts of chlorobenzene by-product formed[25] suggest[23] that under catalyst-free conditions the undesirable free radical activity[26] is favoured. The use of a proper catalyst could turn an oxidation route toward a selective, concerted-like mechanism, at the same time suppressing the free radical activity. However, there is a lack of clear understanding of *m*-CPBA oxidant behaviour and respective reaction

[a] *Centro de Química Estrutural, Instituto Superior Técnico, Universidade de Lisboa, Av. Rovisco Pais, 1049-001 Lisboa, Portugal; E-mail: dmytro.nesterov@tecnico.ulisboa.pt*
[b] *Peoples' Friendship University of Russia (RUDN University), Research Institute of Chemistry, 6 Miklukho-Maklaya st., Moscow 117198, Russia*
[c] *Semenov Federal Research Center for Chemical Physics, Russian Academy of Sciences, ulitsa Kosygina 4, Moscow 119991, Russia*
[d] *Chair of Chemistry and Physics, Plekhanov Russian University of Economics, Stremyannyi pereulok 36, Moscow 117997, Russia*
Electronic Supplementary Information (ESI) available: experimental details, mass-spectra, chromatograms of reaction products and kinetic curves, calculation details. See DOI: 10.1039/x0xx00000x

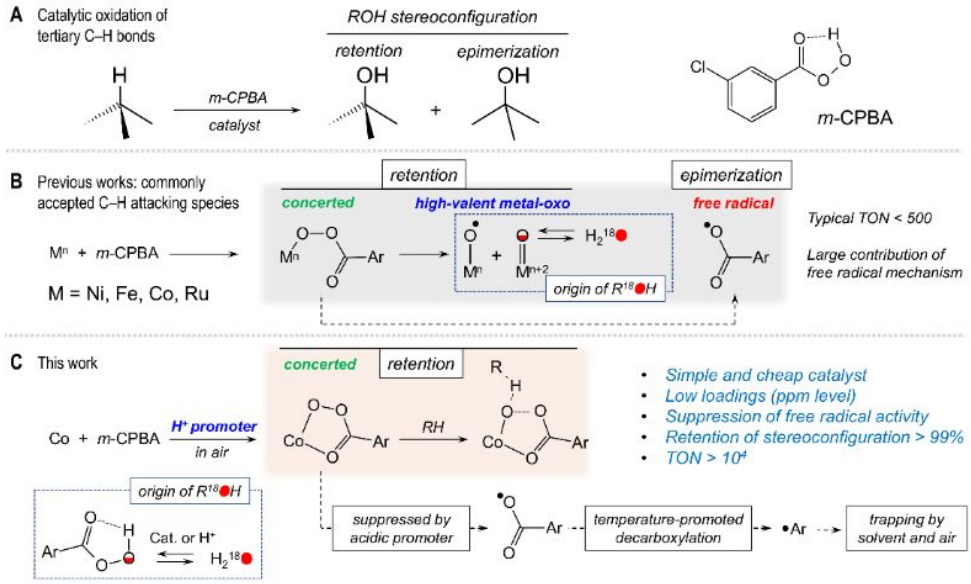

Scheme 1 Hydroxylation of C–H bonds with m-CPBA catalyzed by metal species.

mechanism(s) under catalytic conditions. Although *m*-CPBA, along with PhIO and some other oxidants, is a recognized model oxidant in various metal-catalysed oxidation systems, the respective research trends are typically focused on the investigation of formed metal-containing active species (e.g. HVMO ones),[4, 27, 28] rather than on the chemistry of the oxidant itself. Relatively high bond selectivities, exhibited by O-centred radicals originated from *m*-CPBA, may mislead mechanistic interpretations, where a free radical reaction is interpreted as a HVMO-mediated one.

It is known that *m*-CPBA can react with metal ions to produce highly reactive HVMO species, able to abstract the H atom from inert C–H bonds in a selective manner.[29] The HVMO complexes are of great attention because they are key intermediates in natural enzymatic catalytic systems, including those oxidizing inactive alkanes.[7, 12, 30-32] In turn, *m*-CPBA can serve as a terminal oxidant even in an enzymatic processes, such as oxidation of alkanes catalysed by cytochrome P450.[33] The oxidation potential of *m*-CPBA is sufficient for transforming Fe(III) coordination compounds into highly reactive Fe(IV) and Fe(V) ones, capable of oxidizing strong sp^3 C–H bonds.[34-36] Trivalent ruthenium, being chemically close to iron, has similar behaviour with formation of Ru(IV) and Ru(V) compounds.[37, 38] The power of *m*-CPBA is enough to form Ni^{III}–O(H) and Ni^{III}–O• species from Ni(II) ones,[39-41] what was confirmed by trapping the respective HVMO nickel complexes by ESI-MS and EPR techniques.[40, 41] However, recently Hartwig reconsidered the Ni(II)/*m*-CPBA system, showing that it oxidizes C–H bonds through the free radical mechanism where the aroyloxyl radical ArC(O)O•, but not Ni^{II}–O• or Ni^{III}–O• ones, is responsible for C–H oxidation (Scheme 1).[42]

The early works of Nam demonstrated that compounds of Co(II) and Co(III), in particular porphyrin complex $[Co^{III}(TPFPP)(CF_3SO_3)]$ (TPFPP = *meso*-tetrakis(pentafluorophenyl)porphinato dianion), catalyse oxidation of alkanes and alkenes with *m*-CPBA with a pronounced stereoselectivity.[43, 44] The involvement of cobalt HVMO intermediates was suggested on the basis of high kinetic isotope effect (KIE) of 8 in competitive oxidation of normal and deuterated cyclohexane, as well as incorporation of ^{18}O from $H^{18}O$ into the hydroxylation products (the latter is expected due to $H_2{}^{18}O\cdots M=^{16}O \leftrightarrow {}^{18}O=M\cdots H_2{}^{16}O$ tautomerism, known for M = Fe and Mn; Scheme 1). During our previous studies we obtained similar results (KIE of 7.2) and incorporation of ^{18}O from $H_2{}^{18}O$ using the isoindole compound of cobalt $[Co^{II}(L^1)_2](NO_3)_2$ (L^1 = O,O'-(3-amino-1H-isoindole-1,1-diyl)bis(propan-2-one oxime)), which catalysed hydroxylation of alkanes using *m*-CPBA as a terminal oxidant with >98% retention of stereoconfiguration.[45] In contrast, the complexes of cobalt with acetylacetonate, scorpionate and polypyridyl ligands reveal large contribution of a less selective free radical processes, as demonstrated by Hikichi, Shul'pin and others.[46-49]

The promoting effect of acidic additives is recognized for metal-catalysed oxidations with H_2O_2,[10] but is majorly not known for *m*-CPBA. Recently we have shown that within the range of $[M^{II}(Pc)]$ phthalocyanine complexes having similar structures, cobalt phthalocyanine revealed an exceptional catalytic activity (selectivity and yields of products) of almost one order higher than the other metals studied, when small amounts of nitric acid were used as a promoter.[50] The suppression of the free radical route of *m*-CPBA depends on the acidity (pK_a) of the promoter, as we showed for $[Co^{III}L^2]$ and $[Co^{III}Cd^{II}L^2{}_3Cl_2]$ catalysts (HL^2 = 2-methoxy-6-[(methylimino)methyl]phenol).[51] Another key observation was the difference in incorporations of ^{18}O from $^{18}O_2$ into hydroxylation products when using nitric or acetic acid promoters, that correlated with the overall selectivity using $[Co^{III}Zn^{II}L^2{}_3Cl_2]$ as catalyst.[52] Although the Co/H^+/*m*-CPBA catalytic combination is among the most efficient ones for activation of *m*-CPBA so far, the factors that influence its behaviour as well as the details of the catalytic mechanisms are still to be established. Another open question is the participation of Co(IV) HVMO species in the reaction mechanism, which are known to be elusive due to very high reactivity.[53-55]

In the present work we have found that the heterometallic pre-catalyst $[Co_4Fe_2O(Sae)_8]\cdot 4DMF\cdot H_2O$ (**1**)[20], where H_2Sae = salicylidene-2-ethanolamine, in the presence of an acidic promoter and *m*-CPBA oxidant, affords yields of hydroxylation products up to 70% with the yields of chlorobenzene less than 1%, keeping >99% of retention of stereoconfiguration of model substrates, with TONs (turnover numbers) $>10^4$ and TOF (turnover frequency) up to 2 s^{-1} (Scheme 1). Being interested in establishing of the mechanism of action and optimization of the reaction conditions, we conducted a detailed combined kinetic/^{18}O-labeling/ESI-MS/DFT study that is reported herein.

Results and Discussion

Pre-catalyst 1

The coordination compound $[Co^{III}_4Fe^{III}_2O(Sae)_8]\cdot 4DMF\cdot H_2O$ (**1**) is a hexanuclear complex (Figure 1),[20] where the cobalt centres are coordinated by two Schiff base ligands (deprotonated form of salicylidene-2-ethanolamine, H_2Sae) to form $[Co(Sae)_2]$ fragments, joined by iron centres and an oxygen bridging atom. The outstanding catalytic performance of **1** in the oxidation of alkanes with H_2O_2, as well as the promising results of the activity using *m*-CPBA as an oxidant,[20] inspired us for further studies of the complex **1** as a pre-catalyst.

Kinetic, selectivity and isotopic labeling observations

Retention of stereoconfiguration of a substrate is an important indicator for oxidation mechanisms proceeding without the formation of a free alkyl radical.[56] Thus, we have started the initial studies using *cis*-1,2-dimethylcyclohexane (*cis*-1,2-DMCH), a recognized benchmark substrate[56-59] in stereospecific hydroxylation investigations (Scheme 2).The use of this simple substrate allows collection of stereo- and bond selectivities data simultaneously (apart from the enantioselectivity, which was not the aim of the present study). Starting with simplified models (such as *cis*-1,2-DMCH, methylcyclohexane, etc) concerns a typical approach in the investigation of novel catalytic systems having a complex behaviour. The main aim of this strategy, which is also used in the enzymatic oxidation studies,[60-62] is to understand the principal features, abilities and limitations of the catalytic system and to distinguish between free radical and other types of reaction mechanisms. In the chosen model system, chlorobenzene and *m*-chlorobenzoic acid are common by-products formed from *m*-CPBA (chlorobenzene is formed through the rapid elimination of CO_2 from *m*-chlorobenzoate radical, which is a product of homolytic splitting of the *m*-CPBA O–O bond to generate the acyloxyl radical[23]).

As the heterometallic coordination compound $[Co_4Fe_2O(Sae)_8]\cdot 4DMF\cdot H_2O$ (**1**) was found to be a pre-catalyst (see below), producing catalytically active cobalt species $[Co(Sae)_2]^+$ upon dissolution (see below), all the respective concentrations, TON and TOF values will be given using quadruple concentration of the complex **1** (i.e. $[\mathbf{1}_{Co}] = 4[\mathbf{1}]$).

Addition of *m*-CPBA (0.045 M; here and further the concentrations concerning the final catalytic solutions are given) to an acetonitrile solution of **1** (with $[\mathbf{1}_{Co}]_0 = 1.2 \times 10^{-4}$ M), HNO_3 (5.5×10^{-3} M) and *cis*-1,2-DMCH (0.1 M) afforded the tertiary *cis*-alcohol as the main reaction product, with the ratio of concentrations of tertiary *cis* : *trans* alcohols (*c*/*t* ratio) of 56 (corresponds to >99% of retention of stereoconfiguration; see SI) after 1 h reaction time (Table 1, Entry 1) and 46% of yield of hydroxylation products based on *m*-CPBA, which is in deficit. With a reduced amount of *cis*-1,2-DMCH (0.025 M) and *m*-CPBA (0.027 M) the yields based on *m*-CPBA can be improved up to 56% (Entry 2), keeping a high *c*/*t* ratio. By lowering the catalyst concentration, TON (turnover number, mols of product per mol of catalyst) and TOF (TON per second) values of 1.4×10^4 and 1.8 s^{-1}, respectively, were reached (Entry 3). Furthermore, the yield of chlorobenzene dropped below 1 %. The combination of *m*-CPBA and HNO_3 is a crucial point for the present catalytic system: only traces of *cis*- and *trans*-alcohols (with *c*/*t* ~ 1) were detected when peracetic acid, benzoyl peroxide or its combinations with H_2O_2 were used as oxidants. Further, low yields of tertiary products with *c*/*t* ratio of only 2 were observed in the absence of HNO_3 promoter (Table 1 Entry 6). Only traces of tertiary alcohols were detected in the absence of the pre-catalyst **1**, with no stereoselectivity observed (Entry 7).

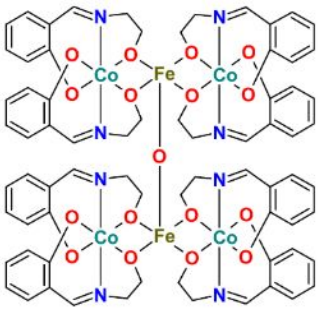

Figure 1. Schematic representation of the structure of **1** in the solid state. Uncoordinated DMF and water molecules are omitted for clarity.

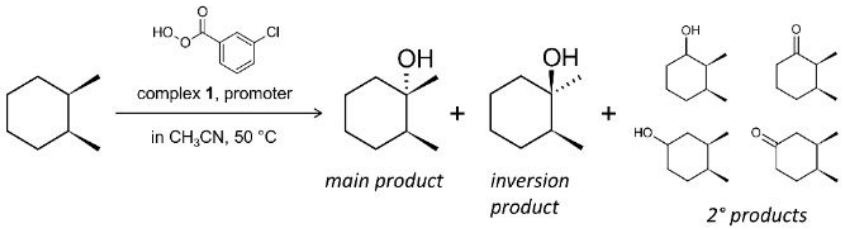

Scheme 2 Model reaction for the study of catalytic and mechanistic features of the **1**/HNO_3/*m*-CPBA system: oxidation of *cis*-1,2-dimethylcyclohexane (*cis*-1,2-DMCH). Only one enantiomer of each tertiary alcohol is shown for clarity

Table 1. Catalytic activity of **1** and *in situ* constructed systems in oxidation of *cis*-1,2-DMCH[a]

Entry / Catalyst[b]	Yields of hydroxylation products[c]		Yield of chlorobenzene[d]	TON[e]	Initial rate W_0[f]	TOF[g]	c/t[h]	RC[i]	3° : 2°[j]
	tertiary *cis*-alcohol	Total							
1 / **1**[k]	42	46	1.3	176	7.1×10^{-5}	0.6	56	99.7	37
2 / **1**[l]	48	56	1.8	1.4×10^{3}	1.2×10^{-5}	1.1	52	99.9	30
3 / **1**[m]	62	72	0.8	1.4×10^{4}	2.4×10^{-6}	1.8	41	98.7	31
4 / **1**[n]	42	47	0.9	105	8.8×10^{-5}	0.7	51	99.7	47
5 / **1**	53	63	0.7	1.6×10^{3}	1.5×10^{-5}	1.4	37	98.4	34
6 / **1**[o]	12	20	15.6	490	1.4×10^{-5}	1.3	2	37.6	20
7 / catalyst-free test	1.5	2.4	0.1	–	5.8×10^{-8}	–	2.4	24.1	–
8 / **1** under N_2	59	74	5.4	73	9.6×10^{-6}	0.9	14	90.7	34
10 / $Fe(NO_3)_3$[p]	4	9	3.0	150	–	–	2	23.2	8
11 / $Fe(NO_3)_3$[q]	4	6	0.7	102	–	–	2	40.0	19
12 / $Co(NO_3)_2$[r]	23	30	6.7	736	4.9×10^{-6}	0.5	10	84.9	21
13 / $Co(NO_3)_2$[s]	57	65	1.0	1.6×10^{3}	1.4×10^{-5}	1.2	30	97.0	36
14 / Co-Fe-H_2Sae *in situ*[t]	58	68	1.7	166	1.2×10^{-4}	1.0	35	99.8	31
15 / Co-Fe-H_2Sae *in situ*[u]	62	72	1.0	1.9×10^{3}	1.7×10^{-5}	1.5	29	96.8	37
16 / **2**[v]	63	71	0.3	1.7×10^{3}	1.5×10^{-5}	1.4	213	99.1	35
17 / **1**[w]	62	70	0.3	1.7×10^{3}	1.8×10^{-5}	1.6	168	98.8	36

[a] Conditions (for pre-catalyst **1**; see respective entries for other catalysts) unless stated otherwise: $[cis\text{-1,2-DMCH}]_0 = 0.1$ M, $[m\text{-CPBA}]_0 = 0.027$ M, $[HNO_3]_0 = 5.5 \times 10^{-3}$ M, $[\mathbf{1}_{Co}]_0 = 1.1 \times 10^{-5}$ M in CH_3CN (5 mL total volume), 50 °C, open air, data shown are for 1 h reaction time after quenching the probes with PPh_3; [b] special conditions or other catalysts; [c] total yields (%) of the 3° and 2° products based on *m*-CPBA; yields of 3° products are the sums of tertiary *cis*- and *trans*-alcohols; yields of secondary products (2°) are the sums of respective alcohols and ketones; [d] yield (%) of chlorobenzene based on *m*-CPBA; [e] turnover numbers, mols of products (sum of 3° and 2° products) per mol of cobalt metal; [f] reaction rate of tertiary *cis*-alcohol formation at zero time (M s^{-1}); [g] turnover frequency at zero time (s^{-1}), initial rate W_0 per mol of cobalt metal; [h] mols of tertiary *cis*-alcohol per mol of *trans*-alcohol. In the present work, the commercial substrate, *cis*-1,2-DMCH, contained *ca*. 1% of *trans*-isomer, which lowered the final *cis*/*trans* ratio and was accounted when calculating the RC index; [i] retention of stereoconfiguration percentage, calculated as $RC = 100(cis - trans + \rho \cdot cis) / (cis + trans - \rho \cdot cis)$, where *cis* and *trans* designate the concentrations of respective products and ρ is the fraction of *trans*-1,2-DMCH in the commercial *cis*-1,2-DMCH substrate (ρ = 0.018 for Entries 1–15 and 1.6×10^{-4} for Entries 16 and 17); [j] bond selectivity, yields of 3° products / yields of 2° products × 4 (for normalization, since 3° : 2° C–H bonds = 2 : 8 = 1 : 4); [k] $[m\text{-CPBA}]_0 = 0.045$ M, $[\mathbf{1}_{Co}]_0 = 1.2 \times 10^{-4}$ M; [l] $[cis\text{-1,2-DMCH}]_0 = 0.026$ M; [m] $[\mathbf{1}_{Co}]_0 = 1.4 \times 10^{-6}$ M, 3 h; [n] $[\mathbf{1}_{Co}]_0 = 1.2 \times 10^{-4}$ M; [o] no HNO_3 added; [p] $[Fe(NO_3)_3]_0 = 1.6 \times 10^{-5}$ M, no HNO_3; [q] $[Fe(NO_3)_3]_0 = 1.6 \times 10^{-5}$ M; [r] $[Co(NO_3)_2]_0 = 1.1 \times 10^{-5}$ M, no HNO_3; [s] $[Co(NO_3)_2]_0 = 1.1 \times 10^{-5}$ M; [t] subsequent addition of CH_3CN solutions of $Co(NO_3)_2$ and $Fe(NO_3)_3$ to H_2Sae solution (concentrations corresponding to imaginary $[\mathbf{1}]_0 = 3 \times 10^{-5}$ M); [u] the same, corresponding to $[\mathbf{1}]_0 = 2.7 \times 10^{-6}$ M; [v] the complex $[Co^{III}(HSae)(Sae)] \cdot CH_3OH \cdot H_2O$ (**2**) was used as a catalyst (1.1×10^{-5} M); [w] the same conditions as for Entry 5, except of *cis*-1,2-DMCH substrate containing less admixture of *trans*-1,2-DMCH ($\rho = 1.6 \times 10^{-4}$).

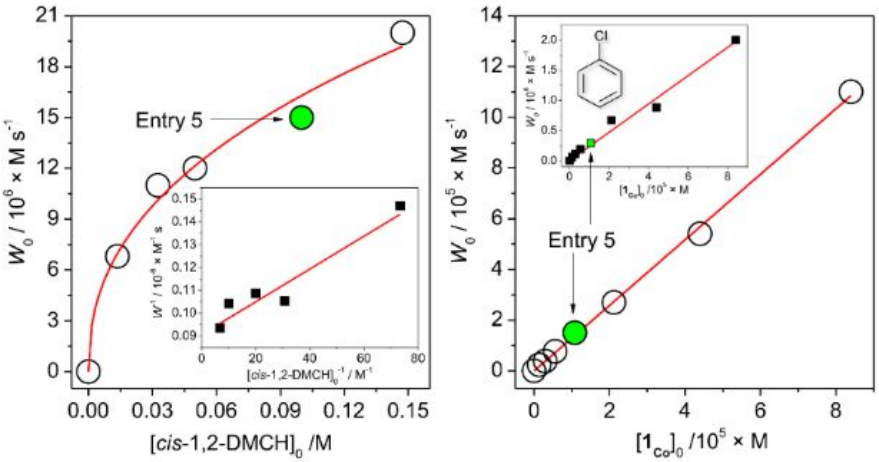

Figure 2. Dependences (experimental points) of the reaction rates (see the SI) of tertiary *cis*-alcohol accumulations on concentrations of substrate (*cis*-1,2-DMCH, left) and **1** (right). Conditions, except of the concentration varied, are as those for Entry 5, Table 1 (solid green circles and squares correspond to Entry 5). Left figure inset shows the linearization of *W vs.* $[cis\text{-1,2-DMCH}]_0$ dependence in reciprocal coordinates (solid line is the linear fit). Right figure inset shows the dependence of the chlorobenzene initial rate formation on $[\mathbf{1}_{Co}]_0$.

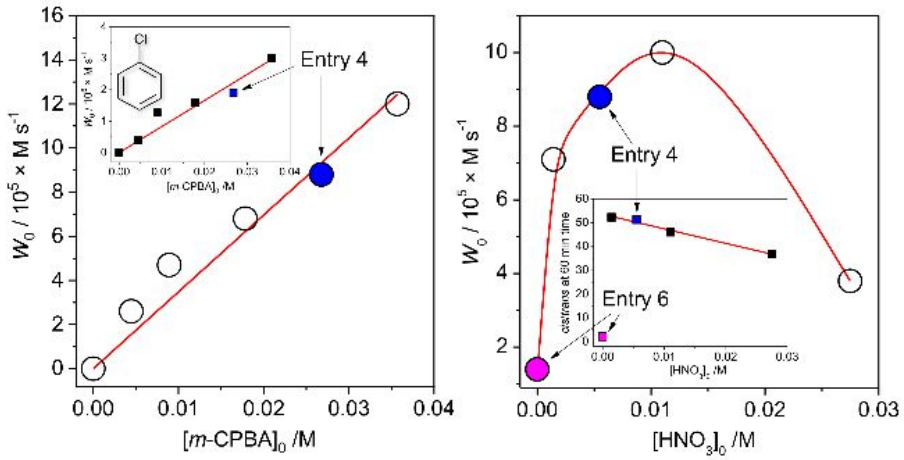

Figure 3. Dependences (experimental points) of the initial reaction rates (see the SI) of tertiary *cis*-alcohol accumulations on concentrations of oxidant (*m*-CPBA, left) and acid promoter (HNO_3, right). Conditions, except of the concentration varied, are as those for Entry 4, Table 1. Left inset shows the dependence of the initial rate of chlorobenzene accumulation on concentration of oxidant. Right inset shows the dependence of achieved (at 60 min reaction time) *c*/*s* ratio on concentration of acid promoter (solid line shows the linear fit of the data for [HNO_3]$_0$ > 0 M region). Solid blue and magenta circles and squares correspond to conditions of Entries 4 and 6, Table 1, respectively.

The dependence of the initial reaction rate W_0 on [*cis*-1,2-DMCH]$_0$ shows a non-linear character without reaching saturation at the concentrations studied (Figure 2, left). The dependence of W_0 *vs*. [**1**$_{Co}$]$_0$ is linear in the range 0 < [**1**$_{Co}$]$_0$ < 8 × 10^{-5} M (Figure 2, right), indicating that no aggregation of active species occurs in solution at these concentrations.[20, 63] The initial reaction rate of chlorobenzene formation shows also a nearly linear dependence on [**1**$_{Co}$]$_0$ (Figure 2, right, inset), suggesting that chlorobenzene is a by-product formed within the main catalytic cycle. The W_0 *vs*. *m*-CPBA dependence shows a behaviour (Figure 3, left) which can be approximated as a linear one. The initial rates of chlorobenzene formation (Figure 3, left, inset) also exhibit a linear dependence. These dependences indicate that alcohol and chlorobenzene molecules are catalytically formed from the *m*-CPBA molecule, but not through the radical chain reaction (for which the non-linear curves are expected). The nitric acid promoter shows a complex dependence (Figure 4, right) of W_0 *vs*. [HNO_3]$_0$ with a marked maximum at [HNO_3]$_0$ = 0.011 M ([HNO_3]$_0$ / [**1**$_{Co}$]$_0$ = 90). The excess of acid promoter led to pronounced suppression of reaction rate and afforded lower *c*/*t* ratios (Figure 3, right, inset). It is clear from this plot (Figure 3, right) that the presence of the nitric acid causes a strict promoting effect on the reaction rate, comparing to acid-free conditions.

From the above set of data, the catalytic conditions with [**1**]$_0$ = 2.7 × 10^{-6} M (*i.e.* [**1**$_{Co}$]$_0$ = 1.1 × 10^{-5} M), [HNO_3]$_0$ = 5.5 × 10^{-3} M, [*m*-CPBA]$_0$ = 0.027 M and [substrate]$_0$ = 0.1 M were chosen for further studies, due to the moderate reaction rate of W_0 = 1.6 × 10^{-5} M s^{-1} (for *cis*-1,2-DMCH) and suitable yields/TON values (Entry 5, Table 1).

While the accumulation of tertiary *cis*-alcohol (retention of stereoconfiguration) shows an expected gradual behaviour (Figure 4, left), the respective dependence of *trans*-alcohol concentration on time (Figure 4, middle) is drastically different: some amount of *trans*-alcohol, formed in the first seconds of reaction, decreases to about half within 1 h reaction time. The commercial substrate (*cis*-1,2-DMCH) was found to contain only trace amounts of both *cis*- and *trans*-alcohols, *i.e.* the observed

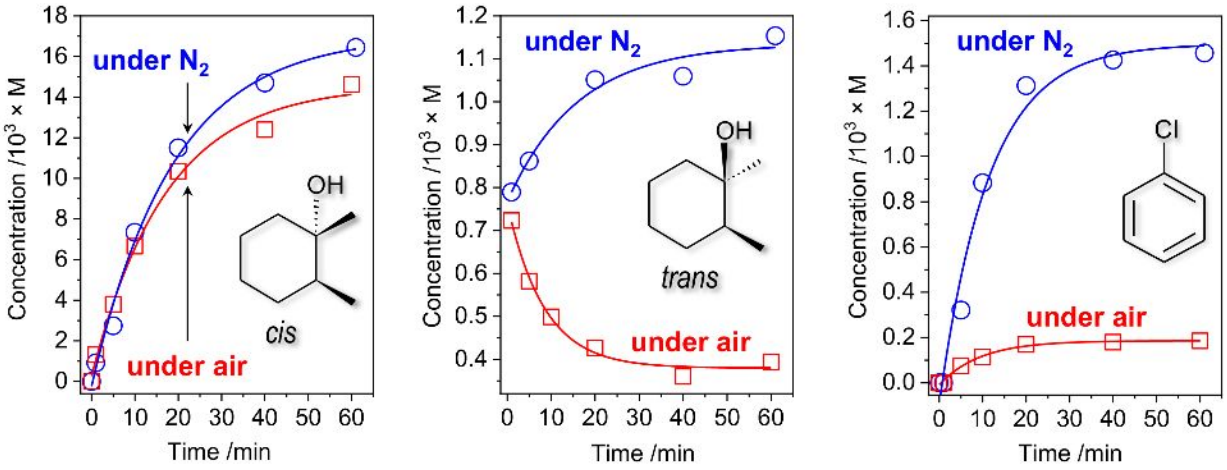

Figure 4. Accumulations of tertiary *cis*-, *trans*-alcohols and chlorobenzene under air (red squares) and N_2 (blue circles) in the course of *cis*-1,2-DMCH oxidation with [*cis*-1,2-DMCH]$_0$ = 0.1 M, [*m*-CPBA]$_0$ = 0.027 M, [HNO_3]$_0$ = 5.5 × 10^{-3} M, [**1**$_{Co}$]$_0$ = 1.1 × 10^{-5} M in CH_3CN (5 mL total volume). Data of Entries 5 and 8, Table 1, are included.

trans-alcohol comes from the catalytic process. Hence, *two reaction steps can be elucidated*: fast initial (first seconds; rapid accumulation of small amounts of both *cis*- and *trans*-alcohols) and then continuous (gradual decrease of *trans*-alcohol and accumulation of *cis*-alcohol amounts) ones. The decrease of *trans*-alcohol concentration can be explained by overoxidation. The observation of the fast initial step does not indicate the formation of CoO_x nanoparticles, as the latter process is typically manifested by a pronounced (up to tens of minutes) lag period.[64]

In the absence of air oxygen, the *trans*-alcohol concentration increases with time, while the accumulation of *cis*-product is not significantly influenced (Figure 4, middle and left). This results in the lower *c*/*t* ratio of 14.3, observed in the absence of O_2 (Entry 8, Table 1). Further, elevated amounts of chlorobenzene (up to 8 times compared to the tests in the presence O_2) were observed in the reaction under N_2 atmosphere (Figure 4, right). The test under atmosphere of pure O_2 showed nearly the same yields and *c/t* ratios as a simple open-air reaction (Entry 9, Table 1).

The reaction by-products during the oxidation of *cis*-1,2-DMCH are those appearing from the attack to secondary C–H bonds (Scheme 2) while products of methyl group oxidation are not detected at all. In the oxidation of *cis*-1,2-DMCH the normalized 3° : 2° selectivity was found to be up to 47 : 1. The overoxidation products are ketones formed through ring cleavage (Figures S11, S19 and S20). Attempt to oxidize various substrates (Scheme 3, A; here and further the conditions are as for Entry 5, Table 1) revealed a pronounced sensitivity of the catalytic system to the position of tertiary R_3C–H bond and nature of the substituent R. The stereospecificity is retained for the oxidation of *cis*-decahydronaphthalene and *cis*-1,4-dimethylcyclohexane, where the *c/t* ratios of the tertiary alcohols of 81 and 38, and the normalized 3° : 2° selectivities of 55 : 1 and 21 : 1 are achieved. The *t*/*c* ratios for *trans*-1,2-dimethylcyclohexane and *trans*-decahydronapthalene were found to be 65 and 63, respectively. Although the total yields (44 and 67%, respectively) are close to those for *cis*-substrates, the selectivity towards tertiary C–H bonds is lower (yields are 33 and 44%), as reflected by the 3° : 2° selectivities of 12 and 15, respectively.

The oxidation of adamantane gave a normalized 3° : 2° selectivity of 20 : 1. The oxidation of 2,3-dimethylbutane (Scheme 3A) proceeded with slightly lower initial reaction rate (9.6×10^{-6} M s^{-1}) comparing with the oxidation of *cis*-1,2-DMCH (1.6×10^{-5} M s^{-1}, Entry 5), resulting in a close yield. Surprisingly, oxidation of cumene (Scheme 3A), which C–H bond dissociation energy (BDE) is considerably lower than that of 2,3-dimethylbutane (97 and 85 kcal mol^{-1}, respectively[65]) gave a reaction rate of only 2.5×10^{-6} M s^{-1} under the same conditions. In the latter reaction about 1% of acetophenone was detected (starting cumene was free of this product), which makes ca. quarter part of the overall yield of products (Scheme 3A). Formation of acetophenone through four-electron oxidation of cumene was observed earlier with ruthenium complexes as catalysts (operating via Ru^{IV}=O HVMO species).[66, 67] The 2,2,4-trimethylpentane reacted weakly, showing only little prevalence for its tertiary C–H bond (Scheme 3, A). Oxidation of *n*-heptane revealed no regioselective preference in different secondary C–H bonds. Only traces of phenol were detected in the oxidation of benzene. Hence, the catalytic system **1**/HNO_3/*m*-CPBA shows pronounced preference for oxidation of tertiary C–H bonds, only slightly reacting with secondary C–H bonds. It is almost totally unreactive towards oxidation of methyl groups and aromatic H atoms.

^{18}O-studies

To gain a further insight, tests using ^{18}O labeled dioxygen and water have been performed in the oxidation of *cis*-1,2-DMCH. The incorporations of ^{18}O from $^{18}O_2$ into tertiary *cis*- and *trans*-alcohols were found to be quite different: while the main product, *cis*-alcohol, contained *ca*. 1% of ^{18}O after 1 h reaction time, the inverted *trans*-alcohol accumulated almost 30% of ^{18}O (Scheme 3, B). The absolute amounts of both labeled tertiary alcohols were comparable (Scheme 3, B). Small amounts of $H_2{}^{18}O$, formed from $^{18}O_2$, were detected. The main reaction product, *cis*-alcohol, incorporates up to 1.6% ^{18}O oxygen from $H_2{}^{18}O$, Scheme 3 B,), while the ^{18}O levels in the *trans*-alcohol are too low for their reliable determination, although one can suppose that the *trans*-alcohol also contains some amounts of ^{18}O (Figure S13). The fragments of 130 *m/z* chromatograms (Scheme 3, B, centre) visually demonstrate that ^{18}O from $H_2{}^{18}O$ preferably goes to *cis*-alcohol, while that from $^{18}O_2$ goes to both alcohols nearly equally. No oxygen exchange between tertiary DMCH alcohols and water was detected within 1 h time in acetonitrile in the presence of nitric acid (Figure S6).

Oxidation of 2,3-dimethylbutane in the presence of 0.5 M $H_2{}^{18}O$ resulted in 2.7% of ^{18}O-labeled alcohol after 1 h (under conditions similar to that for Entry 5, Table 1). However, the respective alcohol (2,3-dimethyl-2-butanol) was found to exhibit slow oxygen exchange with $H_2{}^{18}O$ during the 1 h time period (*ca*. 1% of ^{18}O was detected in a comparative test; see the SI). Hence, we can only say that the ^{18}O incorporation in the course of catalytic process may contribute to the final ^{18}O levels. Oxidation of cumene in the presence of 0.5 M $H_2{}^{18}O$ resulted in 49% ^{18}O enrichment of cumene alcohol and 29% of acetophenone, while the products of a phenyl group hydroxylation remained ^{18}O-free. Such a large incorporation of labeled oxygen into cumene alcohol could be explained by the direct oxygen exchange between its hydroxy-group and water. The respective test revealed 13% of ^{18}O-labeled cumene alcohol after 24 h stirring in acetonitrile in the presence of 5.5×10^{-3} M nitric acid.

It was found that ^{18}O from $H_2{}^{18}O$ may appear in alcohols under catalyst-free conditions. The reaction rate exhibited for $[m\text{-CPBA}]_0$ = 0.027 M in the absence of a catalyst is too low (Entry 7, Table 1) for reliable determination of the small ^{18}O levels in the products. With elevated concentrations of $H_2{}^{18}O$ (1.0 M) and *m*-CPBA (0.14 M), in the presence of HNO_3 (5.5×10^{-3} M) and no catalyst, the 4.6% total yield of tertiary alcohols (based on the substrate) was achieved, with *c/t* ratio of 4.8,

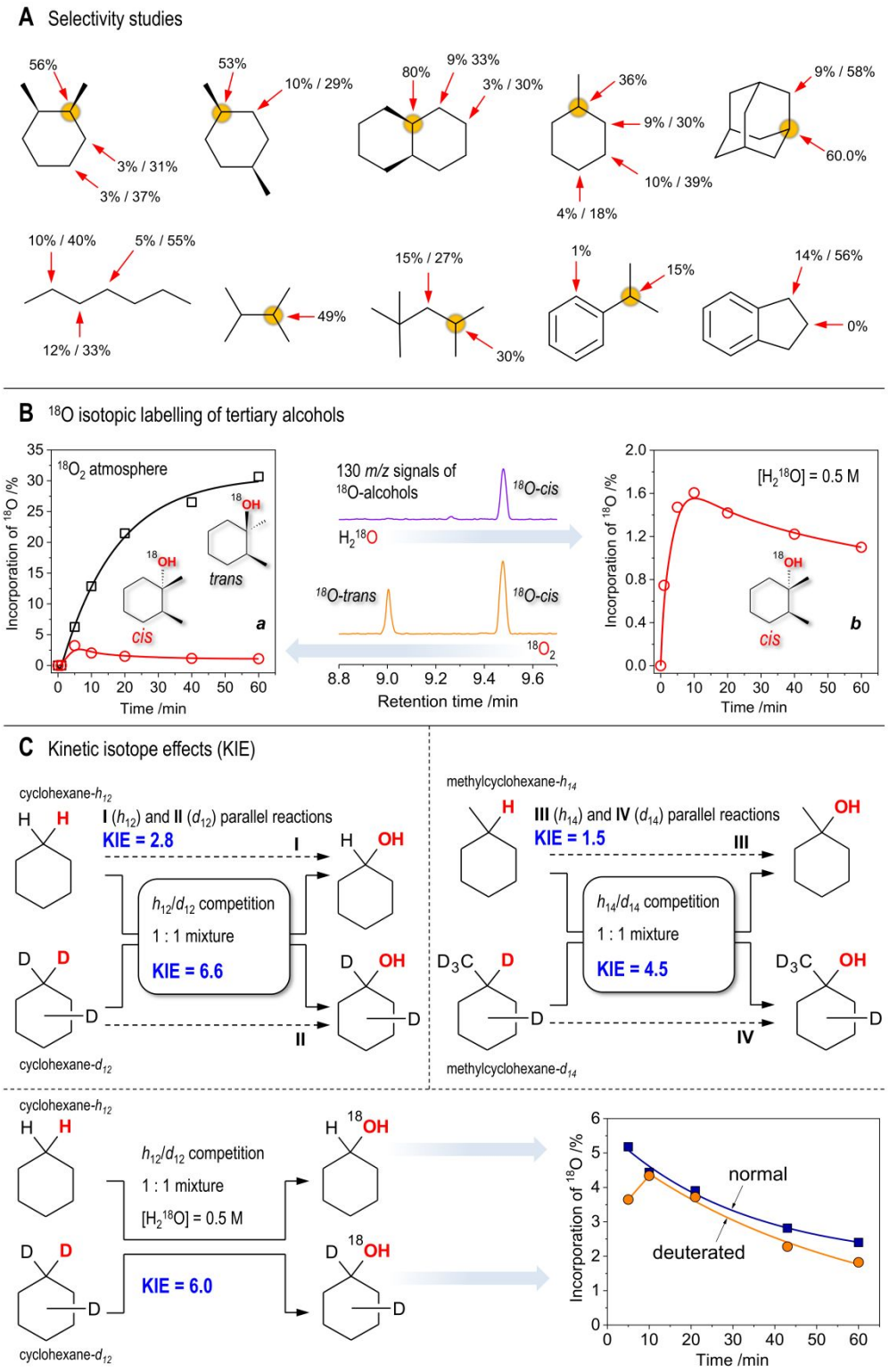

Scheme 3. Key experimental observations. All the conditions correspond to those for Entry 5, Table 1, unless stated otherwise. **A**: bond (3° : 2° C–H bonds) and regioselectivity studies (the latter concerning the 2° C–H bonds oxidation) for selected substrates, shown as the yields of respective products based on substrates / selectivities towards alcohols (yield of alcohol per total yield of the respective alcohol and ketone). Concentrations of substrates are 0.1 M. **B**: *a* (left): incorporation of ^{18}O into tertiary alcohols from $^{18}O_2$; *b* (right): incorporations of ^{18}O into *cis*-alcohol from $H_2{}^{18}O$ (0.5 M); *centre*: fragments of the MS-chromatograms showing the intensities of 130 *m/z* signal (^{18}O-labeled molecular ion of alcohols) for $^{18}O_2$ and $H_2{}^{18}O$ experiments (60 min reaction time). No labeled *trans*-alcohol is observed in the latter case. **C**: top: observed k_H/k_D kinetic isotope effects in the course of oxidation of pure substrates or their equimolar (0.1 M in total) mixtures (normal and deuterated cyclohexane and methylcyclohexane). Bottom: incorporation of ^{18}O from $H_2{}^{18}O$ into cyclohexanols in the course of competitive oxidation of normal and deuterated cyclohexanes.

after 6 h (Figure S10). Under these conditions the *cis*-alcohol accumulated with the reaction rate of 1.8×10^{-5} M s^{-1} and gained 6.2% of ^{18}O after 6 h, while no labeled *trans*-alcohol was detected (Figure S10). Remarkably, in the absence of the promoter both tertiary alcohols contained much lower ^{18}O levels (ca. 1%).

Oxidation of cyclohexane (CyH) in air in the presence of 0.5 M $H_2{}^{18}O$ revealed the initial reaction rate W_0 of 6.4×10^{-6} M s^{-1}, yield of products (sum of cyclohexanone and cyclohexanol) of 30% and alcohol/ketone (*A*/*K*) ratio changing from 14 at 1 min to 0.43 after 1 h. The partial reaction constants revealed that cyclohexanol oxidizes 24 times faster than cyclohexane (Figure S14). Oxidation of cyclohexanol is in accord with the above observation, showing relatively high rate $W_0 = 9.6 \times 10^{-6}$ M s^{-1} even for one order lower substrate concentration, $[CyOH]_0$ = 0.01 M (Figure S15). The reaction rate W_0 of 6.2×10^{-6} M s^{-1}, observed in case the same reaction was performed under N_2 atmosphere, is similar to that for open air reaction. The initial reaction rate of chlorobenzene accumulation was considerably higher for oxidation of cyclohexane under inert atmosphere (1.3×10^{-6} *vs.* 3.8×10^{-7} M s^{-1} for N_2 and air atmosphere, respectively). The maximum percentage of ^{18}O-labeled cyclohexanol (5.0%) was observed at 2 min reaction time (Figure S14, right). After that the amount of the labeled cyclohexanol drops until 1.9% at 60 min.

Kinetic isotope effects and D-labeling

The kinetic isotope effect (KIE) was determined (Scheme 3C), at first, from the competitive oxidation of an equimolar mixture of normal and deuterated cyclohexanes (total concentration 0.1 M) with other conditions as for Entry 5, Table 1. The accumulations of all four products (normal and deuterated alcohols and ketones) are shown at Figure S16, the initial reaction rates W_0 were found to be 3.0×10^{-6} M s^{-1} and 4.8×10^{-7} M s^{-1} for oxidation of C_6H_{12} and C_6D_{12}, respectively (Table S1). The behaviour of accumulations of alcohols and ketones is close to that observed for oxidation of normal cyclohexane (Figure S14), pointing that for both C_6H_{12} and C_6D_{12} the alcohols are oxidized much faster than the ketones (Table S1). While the normal alcohol is oxidized 23 times faster comparing to normal alkane, the respective difference for deuterated cyclohexane was found to be considerably higher (63 times). From the reaction rate constants for normal and deuterated cyclohexane oxidation to cyclohexanol one can calculate the KIE value as k_H / k_D, giving 6.6 (Table S1, Scheme 3C). One can also evaluate the KIE_2 for oxidation of cyclohexanol to cyclohexanone, expressed as $k_{2(H)} / k_{2(D)}$ and found to be 2.4. Considering that the concentrations of alcohols undergo rapid changes (Figures S14 and S16), the observed value of KIE_2 has no chemical significance and just demonstrates that KIE_2 is lower than KIE. Finally, we should note that in the present case the KIE value cannot be correctly determined just as a ratio of products concentrations measured at some certain reaction time: the KIE calculated in this way ranges from 2.7 to 5.6 (calculated for alcohols) or from 5.8 to 7.5 (for all products), with the higher values at the beginning of the reaction.

In contrast to the competitive C_6H_{12}/C_6D_{12} oxidation, the KIE obtained from the parallel tests (independent oxidations of pure normal and deuterated cyclohexanes) shows the considerably lower value of 2.8 (Scheme 3, C). The same difference between competitive and parallel oxidations was observed for methylcyclohexane oxidation: while the competitive process (conditions were as those for cyclohexane) shows a notable KIE effect of 4.5 for tertiary C–H bond, the same reactions revealed nearly equal reaction rates with KIE = 1.5 when h_{14}- and d_{14}-methylcyclohexanes oxidized independently (Scheme 3, C).

The oxidation of 0.1 M deuterated methylcyclohexane revealed 7% of labeled deuterated chlorobenzene as a by-product after 5 min (5% after 1 h). Careful evaluation of all the other tests involving D-labeled substrates disclosed the presence of deuterated chlorobenzene by-product in the oxidation of a mixture of h_{14}- and d_{14}-methylcyclohexanes (4%) and deuterated cyclohexane (4%). Furthermore, the catalyst-free oxidation of the C_6H_{12} / C_6D_{12} mixture using $[C_6H_{12}]_0 = [C_6D_{12}]_0$ = 0.05 M, $[HNO_3]_0 = 5.5 \times 10^{-3}$ M, $[m\text{CPBA}]_0$ = 0.027 M afforded 3% of deuterated chlorobenzene and an approximate KIE value of 5.3 after 24 h (Figure S19), with the total yield of 2%. In turn, oxidation of *cis*-1,2-DMCH in the presence of D_2O resulted in the normal chlorobenzene only. The same product was obtained by using d_4-acetic acid as a promoter. Furthermore, the incorporation of D into chlorobenzene from d_{14}-methylcyclohexane did not depend on the atmosphere (air or N_2), presence of nitric acid promoter or quenching of the samples with PPh_3. An increase of $[d_{14}\text{-MeCyH}]_0$ up to 0.2 M (in the absence of HNO_3) resulted in 13% deuteration of chlorobenzene after 1 h. A very high level of chlorobenzene deuteration (57%) was observed when 0.027 M of *m*-CPBA was stirred in CD_3CN (6% of CH_3CN were present) at 50 °C in the presence of $[\mathbf{1_{Co}}]_0 = 1.1 \times 10^{-5}$ M and in the absence of promoter for 1 hour (Figures S4 and S26).

Combined $H_2{}^{18}O$ / D / KIE studies

The incorporation of ^{18}O from $H_2{}^{18}O$ in the course of C6H12/C_6D_{12} equimolar mixture oxidation at 50 °C disclosed that normal and deuterated alcohols accumulate comparable amounts of ^{18}O (Scheme 3C). The KIE value for the first step (6.0), oxidation of alkane to alcohol, was found to be of the same magnitude (6.6) as for reaction in the absence of $H_2{}^{18}O$. Incorporation of ^{18}O within the time is of nearly linear character for both normal and deuterated products, with the maximum of the labeling at the beginning of the reaction of 5.2% (for C_6H_{12}) and of 4.3% at 10 min time (for C_6D_{12}) (Scheme 3C).

Participation of ROOH intermediates

The search towards alkyl hydroperoxides (a typical product in a free radical oxidation of alkanes[11]) was performed by direct monitoring of alkyl hydroperoxides characteristic spectra by GC-MS[68-72] as well as by indirect methods (comparison of the chromatograms taken before and after addition of the reducing agent PPh_3, according to the method developed by Shul'pin[11]). All the chromatograms recorded before and after addition of

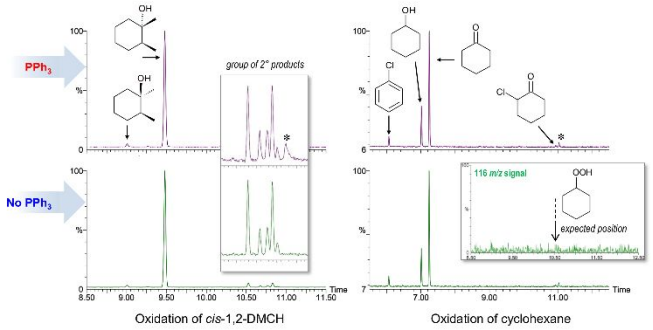

Figure 5. Comparison of the GC chromatograms recorded after (top) and before (below) quenching with solid PPh_3 for oxidation of *cis*-1,2-DMCH (left) or cyclohexane (right). Inset (left) shows the groups of ketones and secondary alcohols formed through the oxidation of the methylenic groups of *cis*-1,2-DMCH. Inset (right) shows the intensity of the 116 *m/z* signal, specific to the mass-spectrum of cyclohexyl hydroperoxide (Figure S23) in the region around to its expected position (10.5 min; Figure S23). Peaks marked by * were not identified.

solid PPh_3 to the probe were identical when the reaction was conducted at 50 °C (Figure 5). No signs for the mass-spectral signal attributable to cyclohexyl hydroperoxide were found (Figure 5, right) even employing a Single Ion Monitoring MS detection mode and lowered reaction temperature (Figure S23). Notably, the chromatograms recorded in the course of *cis*-1,2-DMCH oxidation in the absence of the catalyst (Entry 7, Table 1) at 50 °C reveal significant difference before and after addition of PPh_3 (Figure S11), showing also traces of tertiary alkyl hydroperoxides (Figure S24).

In contrast to the reactions conducted at 50 °C, the chromatograms recorded before and after addition of PPh_3 for 0 °C reactions reveal different patterns (Figures S20 and S21). The yields of products after 2 h time were ca. 5%. The *cis/trans* ratios in the oxidation of *cis*-1,2-DMCH were 15 and 2 before and after addition of PPh_3, respectively. Moreover, the chromatograms recorded before addition of PPh_3 disclosed significant amounts of chlorobenzene, completely disappearing after treatment of the sample with PPh_3 (Figures S20 and S21). The tertiary alcohols did not incorporate ^{18}O neither from $^{18}O_2$ nor $H_2{}^{18}O$ after 2 h at 0 °C reaction, independently on PPh_3. However, the yields of the products as well as the ^{18}O incorporations into the products and CO_2 return to the expected levels when the mixtures were further stirred at 50 °C for 1 h. Samples of the 0 °C reactions injected to GC before treatment with PPh_3 disclose large amounts of CO_2 free of ^{18}O (*ca*. one order higher than those after PPh_3) (Figures S20 and S21). This, together with elevated amounts of chlorobenzene observed before addition of PPh_3, indicates the accumulation of large amounts of aroyloxyl radical ArC(O)O• which undergo rapid decarboxylation when sample passes a hot GC injection zone. However, no peaks attributable to alkyl hydroperoxides were seen neither for oxidation of cyclohexane nor for dimethylcyclohexane.

In situ catalytic system

We attempted to reproduce the catalytic activity of **1** using starting metal salts and their mixtures with the pro-ligand H_2L. Cobalt nitrate exhibits a much lower activity and stereoselectivity than complex **1** (Entry 12, Table 1), whereas iron nitrate was nearly inactive independently of the promoter (Entries 10 and 11). Cobalt nitrate in the presence of nitric acid shows a notable activity (Entry 13), but the stereoselectivity is considerably lower than for the complex **1**, especially for higher $[Co]_0$ (Figure S33). The *in situ* prepared systems (Entries 14 and 15) were found to be active, but showing lower *c/t* ratios (Figures 6 and S33) as compared to the corresponding **1**-based Entries (4 and 5, respectively; Table 1) due to larger production of chlorobenzene and enhanced amounts of *trans*-alcohol.

ESI-MS spectroscopic studies and determination of the putative catalytically active species

Earlier the complex **1** was shown to produce two main types of coordination compounds in acetonitrile solutions: homometallic $[Co^{III}(HSae)_2]^+$ and heterometallic $[\{Co^{III}(Sae)_2\}_2Fe^{III}]^+$ ones (by means of kinetic and ESI-MS methods).[20] Heterometallic species were found to exist only for [**1**] > 5 × 10^{-5} M, while homometallic ones were observed in all studied concentrations. Notably, both species were stable in the presence of a large concentration of the nitric acid promoter (0.04 M).[20] The ESI-MS spectra of the acetonitrile solution of the complex **1** with [**1**] = 4 × 10^{-5} M revealed the presence of $[Co(HSae)_2]^+$ species (387.07 *m/z*, calculated) as a dominant peak (Figure S30) as well as some weaker peaks with higher *m/z* (772.1 and 1243.74, observed), which can be tentatively assigned to $[Co_2(Sae)_4]^+$ and heavier species. After dilution to [**1**] = 2.8 × 10^{-6} M and addition of HNO_3 (5.5 × 10^{-3} M) the $[Co(HSae)_2]^+$ peak remains, while the above peaks disappear. A peak at 166.04 *m/z* (Figure S30) can be attributed to the protonated ligand H_3Sae^+ and this observation allows to presume the existence of equilibrium between coordinated and de-coordinated ligands in solution. The study of an acetonitrile solution of *m*-CPBA revealed a complex pattern in both negative and positive modes (Figure S32). The peaks at 155.33 and 171.35 *m/z* can be attributed to anions of *m*-chlorobenzoic acid (*m*-CBA) and *m*-CPBA, respectively. Addition of a *m*-CPBA acetonitrile solution to the respective solution of the complex **1** with nitric acid (final concentrations equal to that for Entry 5, Table 1) resulted in the appearing of a new peak at 664.45 *m/z* (Figure S30). The latter one, as well as the $[Co(HSae)_2]^+$ at 387.05

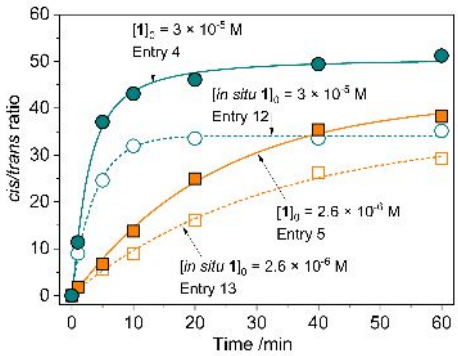

Figure 6. The *c/t* ratios as function of time shown for catalytic systems using pre-catalyst **1** and respective mixtures of salts and ligand (*in situ* systems).

m/z, were found to be short-lived: after 3 minutes the spectra become drastically different, revealing only a low-intensity 168.06 *m/z* signal on a noisy background (Figure S30). This observation could account for the formation of uncharged species, which do not get charged during the ESI-MS experiment. It is proposed that this could be $[Co(HSae)_2(m\text{-CPBA})]^0$ (where *m*-CPBA is in a deprotonated form). From the ESI-MS data and linear W_0 *vs.* $[\mathbf{1}]_0$ relation in the $[\mathbf{1_{Co}}]_0 < 2.5 \times 10^{-5}$ M region the absence of heavier (dimeric) species in catalytic solutions was assumed. The impossibility of detection of neutral species by ESI-MS method is a common case for the catalytic investigations.[73] For instance, similar observations (no ESI-MS detectable species) were reported in the case of olefin epoxidation with the $Co(ClO_4)_2$/*m*-CPBA system.[74] Hence, we concluded that shortly after addition of *m*-CPBA to the reaction mixture all the $[Co(HSae)_2]^+$ species transform to $[Co(HSae)_2(m\text{-CPBA})]^0$ ones, which start the catalytic cycle (see next chapter). This period could be assigned to the initial catalytic phase, when both tertiary *trans*- and *cis*-alcohols are formed in small amounts (see above).

Although decoordination and/or oxidative degradation of the organic ligand in $[Co(HSae)_2]^+$ is possible,[75] we presume this process is negligible in our conditions. Firstly, this species remains stable in the presence of HNO_3 and even H_2O_2.[20] Further, the products of H_2Sae degradation (e.g. salicylic aldehyde) are seen by GCMS method during the alkane oxidation with the HNO_3/H_2O_2 system,[69, 76] but not with the HNO_3/*m*-CPBA one. In the last case they are only detectable if running the **1**/HNO_3/*m*-CPBA system without the substrate for a period of 24 h (Figure S25). No salicylic aldehyde or its oxidation products were detected in regular tests. It is known that treatment of labile cobalt complexes with small amounts of nitric acid in acetonitrile may lead to the formation of the $[Co(CH_3CN)_6]^{2+}$ and $[Co(CH_3CN)_3(NO_3)]^+$ species, which can be seen as 152.3 and 243.5 *m/z* peaks in the ESI-MS spectra.[77] However, in the case of **1**/HNO_3 and **1**/HNO_3/*m*-CPBA solutions no such peaks were detected.

Addition of 1 equivalent (relative to sum of metals) of a strong chelating ligand, 2,2'-bipyridine (bipy), to the reaction mixtures containing **1** ($[\mathbf{1_{Co}}]_0 = 1 \times 10^{-5}$ M) or $Co(NO_3)_2$ ($[Co]_0 = 1 \times 10^{-5}$ M) resulted in complete stereoselectivity loss for **1** (*c*/*t* = 1.5), while the cobalt nitrate catalyst retained significant stereoselectivity (*c*/*t* = 10) (Figure S35). Furthermore, the catalytic system **1** + bipy afforded large amounts of chlorobenzene (18% of yield), while $Co(NO_3)_2$ + bipy system yielded it at 0.4% level only. These results can be understood if one considers interaction of bipy with $[Co^{III}(HSae)_2]^+$ species, leading to catalytically inactive $[Co^{III}(HSae)_2(bipy)]^+$ ones where all positions in the coordination sphere of cobalt are occupied. From the large amounts of chlorobenzene and epimerization of stereoconfiguration of *cis*-1,2-DMCH one may conclude suppression of the stereoselective metal-mediated route and enforcement of the free-radical activity. In contrast, the $[Co(bipy)]^{3+}$ species formed form the cobalt nitrate remain active because they do not contain the chelating ligand other than bipy. Considering that the iron salts were found to be almost unreactive (Entries 10 and 11), and the synthesized

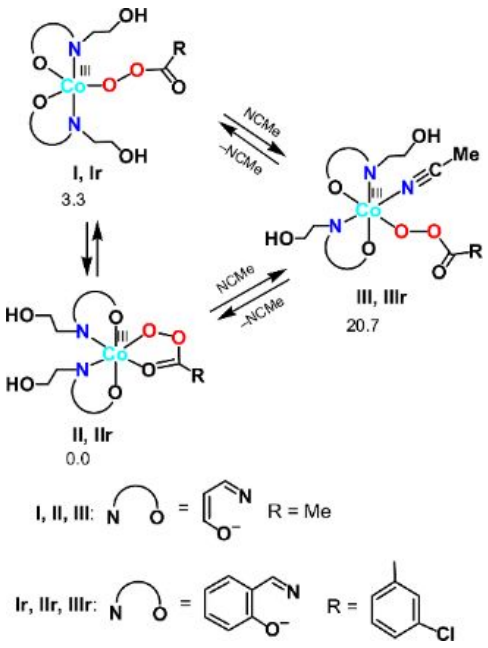

Scheme 4. The calculated most stable isomers of the Co(III) peroxoacidic complexes (relative ΔG_s values for **I**, **II**, and **III** are given in kcal/mol).

model compound $[Co^{III}(HSae)(Sae)]\cdot CH_3OH\cdot H_2O$ (**2**) revealed a catalytic activity similar to that exhibited by **1** (Table 1, Entries 16 and 17; Figures S1 and S36), $[Co^{III}(HSae)_2]^+$ species were further studied as a model of a catalytically active species.

Theoretical mechanistic considerations

(i) Active catalytic species. The plausible reaction mechanism was investigated by theoretical (DFT) methods. The proposed mechanism starts with a degradation of the hexanuclear complex **1** to form, in the presence of the peroxoacid, the Co(III) peroxoacidic complexes $[Co^{III}(HSae)_2\{OOC(O)(m\text{-}C_6H_4\text{-}Cl\}]$ (**Ir**, **IIr**) or $[Co^{III}(HSae)_2\{OOC(O)(m\text{-}C_6H_4\text{-}Cl\}(NCMe)]$ (**IIIr**) (Scheme 4).

First, we analysed the formation of the active catalytic species for peroxoacetic acid taken as a simple model system with a catalyst bearing the 3-iminoprop-1-en-1-ol ligands instead of Sae. All possible geometrical isomers of the corresponding complexes **I–III** were calculated, and only the most stable ones are discussed here (see Schemes 4 and S2 in Supporting Information for the structures and energies of all isomers). The ground state of **II** and **III** was found to be singlet (^{1}**II** and ^{1}**III**) while the ground state of **I** is triplet (^{3}**I**). The calculations indicated that the coordinatively saturated complex ^{1}**II** with the bidentate peroxoacetate ligand is by 3.3 kcal/mol more stable than the penta-coordinated complex ^{3}**I** with the monodentate $MeC(O)O^-$ ligand. On the other hand, formation of complex ^{1}**III** upon addition of one acetonitrile molecule to ^{1}**II** is highly endoergonic (by 20.7 kcal/mol). Thus, namely complex ^{1}**II** may be considered as an active catalytic species.

Based on these preliminary results, the further calculations of the alkane oxidation were carried out for the real oxidant and catalyst used in the experimental part of this work (*i.e. m*-CPBA and **IIr**, Scheme 4).

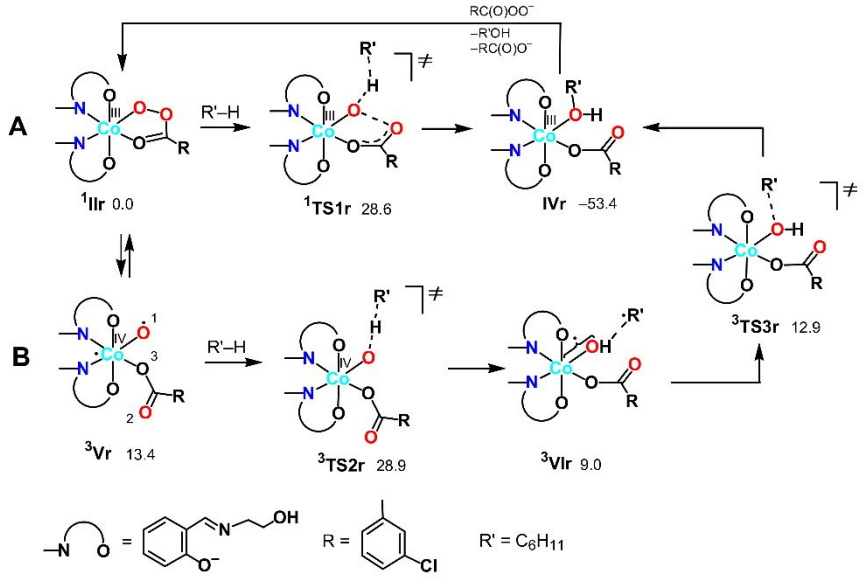

Scheme 5. Possible mechanisms of the alkane (R'H) hydroxylation on the singlet (A) and triplet (B) surfaces (Gibbs free energies in CH_3CN solution are indicated relative to **^{1}IIr** in kcal/mol).

(ii) Closed shell non-radical mechanism. Several possible reaction mechanisms of the cyclohexane (CyH) oxidation were found. In the first mechanism (Scheme 5A), a CyH molecule directly attacks the metal-bound oxygen atom of the peroxo group in the singlet complex **^{1}IIr** to give transition state **^{1}TS1r** (Figure 7). In **^{1}TS1r**, the peroxo O–O bond is partially cleaved (to 2.140 Å) and the C···H···O fragment is significantly bend (to 150.3°). In accord with the IRC calculations, the following evolution of the molecular system is associated with the complete cleavage of the O–O and C–H bonds and formation of the C–O and O–H bonds to give complex $[Co(HSae)_2\{OC(O)R\}(CyOH)]$ (**IVr**) with the coordinated *m*-chlorobenzoate ligand and cyclohexanol molecule. The liberation of CyOH and substitution of $RC(O)O^-$ for $RC(O)OO^-$ in the coordination sphere of the metal complete the catalytic cycle. Thus, this is a one-step non-radical mechanism, and it corresponds to the reductive O–O bond cleavage and to the direct two electron oxidation of alkane by peroxide.

Besides **^{1}TS1r**, another possible transition state with the η^2-coordinated peroxoacid was also found for this mechanism (Scheme S3 in ESI). However, this TS has very high relative energy and, therefore, this possibility may be ruled out.

(iii) Radical rebound mechanism. The second mechanism is based on the homolytic O–O bond cleavage in **IIr** to give a Co oxo-complex which reacts with the alkane C–H bond via the oxygen rebound mechanism (Scheme 5B). The homolytic O–O bond cleavage requires the initial spin conversion of **IIr** from singlet to triplet state. The active catalytic species for this mechanism is complex $[Co(HSae)_2(O)\{OC(O)R\}]$ (**^{3}Vr**) (see ESI for details). Spin density in **^{3}Vr** is localized at the Co and O(1) atoms (0.80 and 1.21 e, respectively, Figure 8) indicating that this species should be better described as the Co^{IV}–O$^\bullet$ (oxyl) complex rather than the Co^{V}=O species. Complex **^{3}Vr** could exchange oxygen with $H_2{}^{18}O$, leading to the ^{18}O-labeled alcohols, in a process known for the high-valent oxo complexes of iron or ruthenium, formed upon reaction with *m*-CPBA.[34, 38, 78, 79]

At the next step, a hydrogen atom of alkane may be abstracted by the oxygen atom O(1) in **^{3}Vr** via **^{3}TS2r** to give the hydroxo complex $[Co(HSae)_2(OH)\{OC(O)R\}]$ (**^{3}VIr**) and cyclohexyl radical loosely bound to the hydroxo ligand. The following rebound of the Cy$^\bullet$ radical leads to complex **IVr** via **^{3}TS3r**. Similar rebound pathways **$^{5/7}$Vr** + CyH → **$^{5/7}$TS2r** → **$^{5/7}$VIr** were found for the quintet and septet surfaces. However, they are more energy demanding that the route on the triplet surface. Several other mechanisms are described in ESI but all of them are less feasible.

(iv) Activation energies. The activation barriers are very similar for both pathways based on **^{1}TS1r** and **^{3}TS2r** (28.6 and 28.9 kcal/mol, respectively). Thus, the calculations indicate that two pathways, *i.e.* non-radical and radical rebound, should occur concurrently and explain the experimentally observed stereoselectivity of the reaction (Figure 9). The first pathway

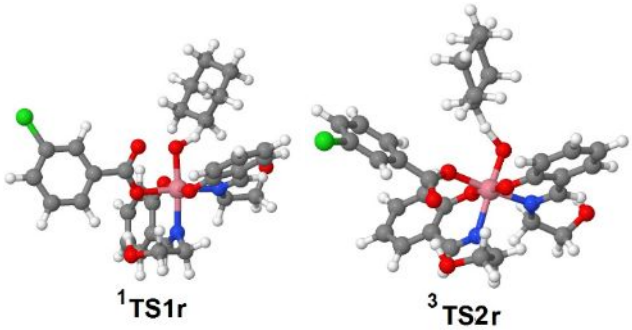

Figure 7. Calculated equilibrium structures of the most important transition states.

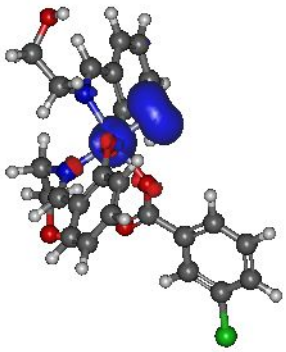

Figure 8. Spin density distribution in **^{3}Vr**.

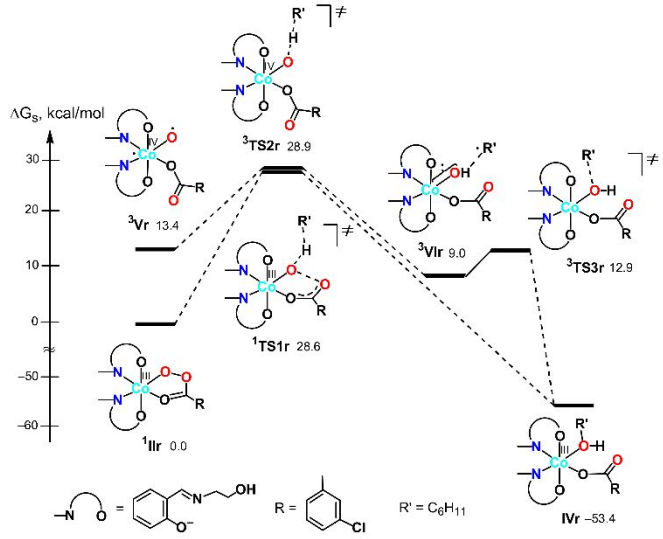

Figure 9. Energy profiles of the most favourable mechanisms of cyclohexane hydroxylation.

results in a complete retention of the substrate stereoconfiguration. The second (rebound) pathway is also typically associated with a high degree of stereoselectivity due to a short lifetime of radicals until their rebound. However, the existence of an activation barrier for the rebound step **VIr** → **IVr** (3.9 kcal/mol) permits some events of the stereoconfigurationinversion accounting for the formation of *trans*-alcohol as a minor product. This mechanistic scheme resembles the literature data on the hydrocarbon hydroxylation with Cytochrome P450 where two low-spin and high-spin pathways with similar energies were proposed and calculated to explain the experimental observations.[80] The energy difference of the low-spin and high-spin pathways and the barrier of the rebound step determine the observed stereoselectivity of the reaction.

Discussion

Let us briefly collect key observations on the **1**/HNO_3/*m*-CPBA system:

(*a*) The system is highly selective towards oxidation of tertiary C–H bonds with high level of retention of stereoconfiguration (RC > 99%) when nitric acid is used as a promoter. The promoters of lower acidity, such as acetic and trifluoroacetic acids reveal lower bond and stereoselectivity.[51, 52]

(*b*) The system is strictly air-sensitive: in the absence of dioxygen the *c*/*t* ratio drops from >60 to 15 due to the elevated yield of the *trans*-product. Large amounts of chlorobenzene are formed in the absence of dioxygen. The catalyst-free system is air-sensitive in the same way.[23]

(*c*) At 50 °C, labeled oxygen incorporates from $^{18}O_2$ mainly to the *trans*-product (up to 30%), giving nearly equal absolute amounts of ^{18}O-tertiary alcohols (*cis*/*trans* ratio < 1.5). Small amounts of $H_2{}^{18}O$ were detected. The incorporation of ^{18}O up to 70% into the *trans*-alcohol was achieved using a Co/Zn complex as a catalyst and a promoter of lower acidity (acetic acid).[52]

(*d*) The labeled oxygen from $H_2{}^{18}O$ incorporates mainly to the *cis*-product; the incorporation level is low (< 2%). The substrate with higher C–H bond energy (cyclohexane) and lower reaction rate gives higher ^{18}O incorporation from $H_2{}^{18}O$. The existence of a metal-free pathway for ^{18}O incorporation from $H_2{}^{18}O$ into the alcohol product under oxidation with *m*-CPBA was disclosed (no direct oxygen exchange between the tertiary alcohols and $H_2{}^{18}O$ was found). Significant amounts of singly and doubly ^{18}O-labeled CO_2 were detected.

(*e*) Nearly equal percentages of ^{18}O come from $H_2{}^{18}O$ into the normal and deuterated alcohols during the competitive oxidation of equimolar C_6H_{12}/C_6D_{12} mixture. Labeled $^{18}OPPh_3$ was detected in the tests with both $^{18}O_2$ and $H_2{}^{18}O$, showing gradual accumulation with time.

(*f*) The kinetic isotope experiments showed considerable KIEs in the competitive oxidations, but a low or negligible KIE in the parallel reactions. The KIE value determined for the catalyst-free system (5.5; competitive oxidation of C_6H_{12}/C_6D_{12}) is of the same magnitude as for the metal-catalyzed one. The KIE value in the competitive oxidation of normal and deuterated cyclohexane is similar to those observed using other cobalt-containing catalysts.[43-45, 51]

(*g*) The formation of 7 to 13 % of deuterated chlorobenzene was accounted for oxidation of d_{14}-methylcyclohexane, containing weak tertiary C–D bonds; no change in D-incorporations into chlorobenzene appears if the reaction is performed under inert atmosphere. The presence of deuterated chlorobenzene was found also in the other tests involving deuterated substrates, but not deuterated additives (D_2O or CD_3COOD). The use of deuterated acetonitrile in the absence of an alkane substrate affords more than 50% of deuterated chlorobenzene. No D-labeled *m*-CBA (*m*-chlorobenzoic acid) was detected.

(*h*) No cyclohexyl hydroperoxide was detected in the cyclohexane oxidation, independently of the atmosphere (air or N_2) and reaction temperature (0 or 50 °C). A separate test showed that cyclohexyl hydroperoxide, if formed, would be stable under the conditions of the experiment (Figure S22). Oxidation of *cis*-1,2-DMCH affords trace amounts of tertiary alkyl hydroperoxides at 50 °C for the catalyst-free reaction. For 50 °C temperature reactions, addition of PPh_3 does not influence the yields and selectivity measured by the GC method.

The main catalytic cycle, confirmed by DFT calculations, proceeds through the formation of [Co^{III}(HSae)$_2$(*m*-CPBA)]

species, indetectable by ESI-MS. Cobalt is believed to maintain its Co(III) oxidation state, but participation of short-lived Co(IV) species is possible (Figure 9, Scheme 6). Although the existence of Co(II) in the presence of a large excess of *m*-CPBA looks not likely, Nam and coworkers suggested that Co(II) retains its oxidation state when mixed with *m*-CPBA, as was shown by EPR studies (the characteristic spectrum with strong transition with g = 4.53 persisted after addition of *m*-CPBA).[74] To verify our hypothesis, the HF-EPR spectrum (256 GHz at 5 K) of a 20 mM solution of the $[Co^{II}(HSae)_2]$ complex in acetonitrile was recorded (Figure S29), featuring a series of transitions typical for Co(II) species (the strongest one with g = 4.51). Addition of 1 equivalent of *m*-CPBA to this solution afforded a considerable decay of the spectrum intensity (Figure S29), thus confirming that cobalt is likely to persist in the Co(III) oxidation state rather than forming the Co(II) one under the conditions of experiment.

We proposed that the C–H oxidation in the Co/*m*-CPBA system proceeds *via* at least two different routes which can be tentatively designated as *selective* and *non-selective* ones (Scheme 6). Basing on our data set, we propose that H abstraction by a chlorobenzene radical **3** is the main basis of a *non-selective* route. Formation of a free alkyl radical R•, which is trapped by O_2 and *m*-CPBA,[11, 42] is the origin of stereoselectivity loss (Scheme 6).

Chlorobenzene radical **3** is reactive enough to attack such a neutral solvent as acetonitrile, thus careful tuning of the solvent nature could enhance stereoselectivity by quenching that radical. The rate of accumulation of chlorobenzene **4** correlates with the promoter acidity.[51] Elevated amounts of chlorobenzene, observed in the absence of O_2, correlate with increased amounts of *trans*- and *cis*-tertiary alcohols. Such influence of dioxygen on the chlorobenzene yield is known for catalyst-free oxidations with *m*-CPBA,[23] thus this process is not regulated by a catalyst. Oxygen readily reacts with carbon-centred radicals, in this way quenching the non-selective free radical process. Oxidation of normal cyclohexane and normal and deuterated methylcyclohexane in the presence or absence of O_2 allows to estimate the relative amount of **3** radical reacting with O_2 (Scheme 6). While the reaction of O_2 with aliphatic C• radicals affords stable COO• ones, the respective reaction with aromatic radicals may afford degradation of an aryl ring with formation of various species (some products were detected in the substrate-free test, Figure S26). Labeled *m*-chlorophenol **5** was detected for some reactions conducted under $^{18}O_2$.[70]

The *m*-CPBA may form two O-centred radicals, aroyloxyl ArC(O)O• (**2**) and aroylperoxyl ArC(O)OO• (**7**), both capable of H-abstraction from C–H bonds. Hydrogen atom transfer to an aroyloxyl radical **2** from a C–H bond gives a free C• radical, leading to the epimerization of stereoconfiguration, what contradicts the observation (*a*). Oxidation of C–D bonds leads to deuterated chlorobenzene **6**, but not *m*-chlorobenzoic acid (observation (*g*)). Thus, under the conditions of the experiment the radical **2** undergoes nearly quantitative decarboxylation and in this way can be ruled out as a C–H attacking species.

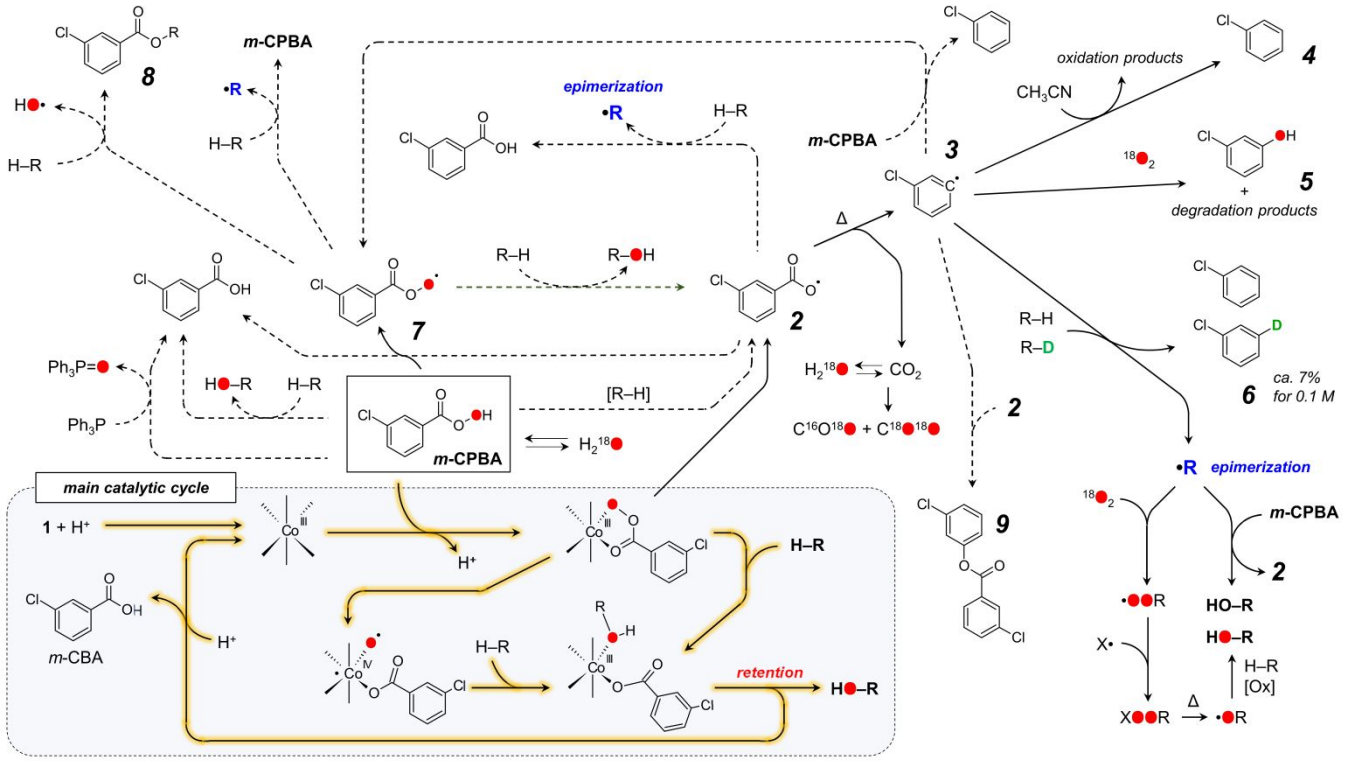

Scheme 6. Proposed reaction pathway. Highlighted solid black lines concern the main cycle. Non-highlighted solid black lines are the main side processes. Dashed lines are possible processes, occurring mainly at low temperature. Participation of water and iron is omitted for clarity.

The interaction of the aroylperoxyl ArC(O)OO• radical **7** with C–H bond is more complicated[23] and may afford various products (Scheme 6), including free aroyloxyl **2** or carbon-centred radical R•, both not supported by the experimental evidences. Another pathway produces an ester **8** as a main product (Scheme 6). The formation of large amounts of alkyl esters (up to 8% based on *m*-CPBA) was accounted for the aerobic autooxidation of adamantane by aldehydes (including *m*-chlorobenzaldehyde),[23, 24] where the RC(O)OO• radical results from the reaction of O_2 with acyl radical RC(O)•. In the case of **1**/HNO_3/*m*-CPBA system, trace amounts of cyclohexyl *m*-chlorobenzoate ester **8** were detected for oxidation of cyclohexane (Scheme 6, Figure S27). These observations suggest that no or only trace levels of the aroylperoxyl ArC(O)OO• radical **7** are formed in the **1**/HNO_3/*m*-CPBA system. The 3° : 2° bond selectivity of the H atom abstraction by the ArC(O)OO• radical from adamantane was evaluated to be 46 : 1 and 78 : 1, depending on the method of generation of an acyl radical (photosplitting of benzyl[42] or autooxidation of *m*-chlorobenzaldehyde,[23] respectively). These values differ from those observed for adamantane oxidation by Co/HNO_3/*m*-CPBA systems (from 23 : 1 to 39 : 1).[51] The ArC(O)OO• radicals themselves can be obtained from the reaction of acyl radical with O_2 or aroyloxyl radical with *m*-CPBA. Both processes cannot be considered as favourable due to the relatively low concentrations of the respective species. Therefore, participation of the aroylperoxyl ArC(O)OO• radical **7** in the main oxidation route is not likely.

The rate of the catalyst-free oxidation of *cis*-1,2-DMCH under our conditions was evaluated as 6×10^{-8} M s^{-1}. The catalytic effect is clearly seen at 10 ppm level of **1**, while 1000 ppm (0.1 mol%) loading allows ca. 1000-fold increase of the reaction rate. The plausible mechanism of C–H hydroxylation (Figure 9 and Scheme 6) foresees coordination of *m*-CPBA to the cobalt centre with the subsequent O-atom insertion into the C–H bond or transfer to a short-lived alkyl radical (rebound). Observations (*e*) and (*f*) suggest that the hydrogen atom abstraction is rather a product determining than a rate determining step.[81] This conclusion is in accord with the non-linear W_0 *vs*. $[substrate]_0$ dependence (Figure 2), where high concentrations of substrate have less influence on the reaction rate than low concentrations. The strictly linear W_0 *vs*. $[catalyst]_0$ and nearly linear W_0 *vs*. [*m*-CPBA] dependences, as well as the relatively low reaction temperature, rule out the free radical chain mechanism.[82]

The principal reaction pathway (Scheme 6, highlighted black lines) presumes formation of *m*-CBA, but not chlorobenzene as a main product of *m*-CPBA transformation. The amount of *m*-CBA found for Entry 5 (Table 1) is 0.02 M, which is very close to 0.017 M expected for the sum of tertiary and secondary hydroxylation products (Figure S34). The difference between these values could be explained by the formation of unaccounted overoxidation by-products as well as by the elevated analytical error in the *m*-CBA quantification due to GC peak broadening. The sum of concentrations of substrate and hydroxylation products was 0.1 M during the catalytic run (Figure S34). Similar results were obtained for the oxidation of *trans*-decahydronaphthalene (a less volatile substrate than *cis*-1,2-DMCH), for which the sum of substrate and products was roughly 0.1 M after 1 h (the sum of products was 0.018 M and amount of *m*-CBA formed was 0.019 M). Therefore, the overall mass balance of the reaction is retained.

The role of iron in the overall catalytic cycle appears to be more hidden. The only detected iron-containing species in a solution of **1** is $[\{Co^{III}(Sae)_2\}_2Fe^{III}]^+$.[20] The latter, however, exists for [**1**] > 1×10^{-5} M, and at lower concentrations of **1** the iron species possibly exist in solvated Fe(III) forms and complexes with *m*-CBA (*m*-chlorobenzoic acid) and *m*-CPBA. Compounds of iron could serve as highly selective catalysts when using *m*-CPBA oxidant, presumably operating through the Fe(IV) or Fe(V) HVMO species.[34, 35, 59] However, as the stabilization of HVMO species typically requires electron-rich N-donor polypyridyl, cyclam or similar ligands,[4] their appearance is not likely. In the absence of such ligands, iron catalysts demonstrate low reactivity with *m*-CPBA and mainly induce low-selective processes (Table 1, Entries 10 and 11). On the other hand, Fe(III) species are known to react with free O- and C-centred radicals in the course of a Fenton-like reaction.[11, 26, 83] Therefore, the small amounts (ca. 5×10^{-6} M in a typical test) of Fe(III) species in the **1**/HNO_3/*m*-CPBA catalytic system should not interfere with the main reaction pathway, but would trap and neutralize free-radicals, responsible for low-selective C–H oxidation (Scheme 6), in this way enhancing the overall selectivity.

The incorporations of ^{18}O from $H_2{}^{18}O$ into the alcohols at < 10% level, observed for plenty of Co/*m*-CPBA catalytic systems as well as for the **1**/HNO_3/*m*-CPBA one, require further comment. Appearance of oxygen from water in the course of a metal catalysed oxidation with a peroxide is usually considered as an evidence for HVMO species, because the latter may exchange oxygen with water.[84-87] A free radical reaction mechanism (*e.g.*, with the HO• radical as the C–H attacking species) does not afford labeled alcohols. Although observation of ^{18}O in alcohols and epoxides in the M/*m*-CPBA (M = transition metal) systems was often interpreted as a HVMO oxygen exchange,[36, 38, 43-45, 88, 89] a metal-free oxidation of *cis*-1,2-DMCH by *m*-CPBA in the presence of $H_2{}^{18}O$ and nitric acid promoter readily resulted in ^{18}O-labeled tertiary *cis*-alcohol (Figure S10), pointing out the existence of an ^{18}O-incorporation mechanism alternative to a HVMO one (the possibility of a direct oxygen exchange between tertiary *cis*-alcohol and water under the typical conditions of the experiment was ruled out, see the SI). Direct labeling of *m*-CPBA (Scheme 6) could explain the appearance of ^{18}O from $H_2{}^{18}O$ in all cases. Transfer of a peroxyl oxygen from *m*-CPBA and aroylperoxyl radical **7** to C–H bond and PPh_3 (Scheme 6) suggests that this oxygen atom is already ^{18}O-labeled prior to C–H hydroxylation. Nearly equal incorporations of ^{18}O into normal and deuterated alcohols (observation (*e*)) fit with this assumption. Reaction of PPh_3 with labeled *m*-CPBA results in $^{18}OPPh_3$, which accumulates in all tests involving $H_2{}^{18}O$ (Figure S28). Appearance of $^{18}OPPh_3$ in the tests in the $^{18}O_2$ atmosphere can be explained by reduction of $^{18}O_2$ to $H_2{}^{18}O$. This process was confirmed by observation of

labeled ketones and CO_2 (Figures S20 and S21). Considering the rather low incorporations of ^{18}O into the alcohols (less than 5%), the magnitude of the oxygen exchange rate between *m*-CPBA and $H_2{}^{18}O$ can be evaluated to be *ca*. one order lower than for C–H hydroxylation (under the studied conditions). This also explains why substrates with higher C–H bond energy, showing lower oxidation rate, get higher ^{18}O-enrichment.

Conclusions

In conclusion, we have studied the catalytic reaction mechanism of the stereospecific oxidation of saturated hydrocarbons using *m*-chloroperoxybenzoic acid (*m*-CPBA) as oxidant, a Co/Fe heterometallic complex as a pre-catalyst and nitric acid as a promoter. The combination of a protic promoter with the cheap cobalt-based catalyst is essential for the pronounced catalytic effect and unusual stereoselectivity that concerns a main novelty. The proposed catalytic system hydroxylates tertiary sp^3 C–H bonds with retention of stereoconfiguration up to 99%, achieving exceptionally high TONs (up to 1.4×10^4) and reaction rates (TOFs up to 2 s^{-1}). The typical catalyst loading is 1000 ppm, but the system can efficiently work even at ppm loadings. A reaction temperature of 50 °C facilitates the solubility of the hydrocarbon substrates, at the same time favouring decarboxylation and further degradation of aroyloxyl and aryl radicals, which are responsible for the non-selective free radical side pathway (less than 1% of *m*-CPBA transforms into chlorobenzene under the conditions of experiment). The latter free radical activity is also efficiently hampered by a protic acid promoter.

DFT calculations and selectivity studies, as well as D- and ^{18}O-labeled experiments, indicate that the main reaction mechanism involves a metal^{III}-peroxo or a metal^{IV}-oxyl C–H attacking species (the latter being a rebound process), rather than free-radical pathways. Further, despite the large primary kinetic isotope effect up to 6.6 in the competitive oxidations, the H atom abstraction appears to be a product determining, but not the rate determining step in the Co/*m*-CPBA oxidations. The fact that the Co(III) catalyst does not change its oxidation state during the most energetically favoured pathway inspires exploration of the catalytic systems for *m*-CPBA activation comprising redox-inactive cations, such as Al(III), Bi(III) or Y(III), usually considered as unsuitable ones for this type of reactions. Some of us have recently observed a pronounced catalytic activity of the aquacomplexes of these cations in the oxidation of alkanes and olefins with H_2O_2.[90-92] One could expect a similar activity for the *m*-CPBA oxidant, what opens the possibility of using redox-inactive transition and main group metals as metal-ligand cooperation catalysts.

Finally, we have found signs for slow direct oxygen exchange between *m*-CPBA and water in the presence of a proton or a metal complex. As the incorporation of ^{18}O from $H_2{}^{18}O$ into alcohols is commonly used as a mechanistic marker for the involvement of HVMO species (often capable of oxygen exchange with water), we conclude that the results of ^{18}O-tests should be treated cautiously when *m*-CPBA is used as the oxidant.

Author Contributions

O.V.N. and D.S.N. initiated and conceptualised the research; O.V.N. acquired and processed the catalytic data; M.L.K. performed the DFT calculations and wrote the respective part; G.B.S. conducted the preliminary studies that inspired the research and assisted writing the manuscript; O.V.N. and A.J.L.P. discussed and edited the manuscript, A.J.L.P. and G.B.S. acquired funding for the work; D.S.N. designed the research methodology and wrote the main manuscript text. All authors contributed to writing the final version of the manuscript.

Conflicts of interest

There are no conflicts of interest to declare.

Acknowledgements

This work was supported by Fundação para a Ciência e Tecnologia (FCT), Portugal (projects UIDB/00100/2020 of Centro de Química Estrutural, PTDC/QUI-QIN/29778/2017, contracts IST-ID/086/2018 and IST-ID/117/2018) and by the RUDN University Strategic Academic Leadership Program. The High-Field EPR spectra were recorded at the EMR facility of the National High Magnetic Field Laboratory, which is supported by National Science Foundation Cooperative Agreement No. DMR-1644779 and the State of Florida. Authors are grateful to Dr. Andrew Ozarowski (NHMFL) for the EPR measurements and for his EPR fit and simulation software SPIN. Authors acknowledge the IST Node of the Portuguese Network of Mass-spectrometry for ESI-MS measurements. Authors thank for support RFBR according to Research Projects Grant No. 19-03-00142; the Ministry of Education and Science of the Russian Federation (project code RFMEFI61917X0007), as well as by the Initiative Program in the frames of the State Tasks 0082-2014-0004 and 0082-2014-0007 “Fundamental regularities of heterogeneous and homogeneous catalysis”; the Program of Fundamental Research of the Russian Academy of Sciences for 2013–2020 on the research issue of IChP RAS No. 47.16.

References

1. P. Gandeepan, T. Muller, D. Zell, G. Cera, S. Warratz and L. Ackermann, *Chem. Rev.*, 2019, **119**, 2192-2452.
2. L. Ping, D. S. Chung, J. Bouffard and S.-g. Lee, *Chem. Soc. Rev.*, 2017, **46**, 4299-4328.
3. R. R. Karimov and J. F. Hartwig, *Angew. Chem. Int. Ed.*, 2018, **57**, 4234-4241.
4. K. P. Bryliakov and E. P. Talsi, *Coord. Chem. Rev.*, 2014, **276**, 73-96.
5. W. R. Gutekunst and P. S. Baran, *Chem. Soc. Rev.*, 2011, **40**, 1976-1991.
6. G. B. Shul'pin, *Org. Biomol. Chem.*, 2010, **8**, 4217-4228.
7. L. Que and W. B. Tolman, *Nature*, 2008, **455**, 333-340.
8. A.J.L. Pombeiro and M.F.C. Guedes da Silva, *Alkane Functionalization*, Wiley, Hoboken, NJ, USA, 2019.
9. M. M. Diaz-Requejo and P. J. Perez, *Chem. Rev.*, 2008, **108**, 3379-3394.

10. D. S. Nesterov, O. V. Nesterova and A. J. L. Pombeiro, *Coord. Chem. Rev.*, 2018, **355**, 199-222.
11. G. B. Shul'pin, *J. Mol. Catal. A*, 2002, **189**, 39-66.
12. S. Sahu and D. P. Goldberg, *J. Am. Chem. Soc.*, 2016, **138**, 11410-11428.
13. C. L. Sun, B. J. Li and Z. J. Shi, *Chem. Rev.*, 2011, **111**, 1293-1314.
14. S. Kal, S. N. Xu and L. R. Que, *Angew. Chem. Int. Ed.*, 2020, **59**, 7332-7349.
15. A. Gunay and K. H. Theopold, *Chem. Rev.*, 2010, **110**, 1060-1081.
16. R. Kumar, B. Pandey, A. Sen, M. Ansari, S. Sharma and G. Rajaraman, *Coord. Chem. Rev.*, 2020, **419**, 31.
17. K. Ray, F. F. Pfaff, B. Wang and W. Nam, *J. Am. Chem. Soc.*, 2014, **136**, 13942-13958.
18. P. Buchwalter, J. Rose and P. Braunstein, *Chem. Rev.*, 2015, **115**, 28-126.
19. O. V. Nesterova, E. N. Chygorin, V. N. Kokozay, V. V. Bon, I. V. Omelchenko, O. V. Shishkin, J. Titis, R. Boca, A. J. L. Pombeiro and A. Ozarowski, *Dalton Trans.*, 2013, **42**, 16909-16919.
20. D. S. Nesterov, E. N. Chygorin, V. N. Kokozay, V. V. Bon, R. Boca, Y. N. Kozlov, L. S. Shul'pina, J. Jezierska, A. Ozarowski, A. J. L. Pombeiro and G. B. Shul'pin, *Inorg. Chem.*, 2012, **51**, 9110-9122.
21. D. S. Nesterov, V. N. Kokozay, V. V. Dyakonenko, O. V. Shishkin, J. Jezierska, A. Ozarowski, A. M. Kirillov, M. N. Kopylovich and A. J. L. Pombeiro, *Chem. Commun.*, 2006, 4605-4607.
22. H. Hussain, A. Al-Harrasi, I. R. Green, I. Ahmed, G. Abbas and N. U. Rehman, *RSC Adv.*, 2014, **4**, 12882-12917.
23. A. Bravo, H. R. Bjorsvik, F. Fontana, F. Minisci and A. Serri, *J. Org. Chem.*, 1996, **61**, 9409-9416.
24. A. Bravo, F. Fontana, F. Minisci and A. Serri, *Chem. Commun.*, 1996, 1843-1844.
25. H. J. Schneider and W. Muller, *J. Org. Chem.*, 1985, **50**, 4609-4615.
26. A. A. Fokin and P. R. Schreiner, *Chem. Rev.*, 2002, **102**, 1551-1593.
27. M. Oszajca, A. Franke, M. Brindell, G. Stochel and R. van Eldik, *Coord. Chem. Rev.*, 2016, **306**, 483-509.
28. A. R. McDonald and L. Que, *Coord. Chem. Rev.*, 2013, **257**, 414-428.
29. K. Cho, P. Leeladee, A. J. McGown, S. DeBeer and D. P. Goldberg, *J. Am. Chem. Soc.*, 2012, **134**, 7392-7399.
30. J. Hohenberger, K. Ray and K. Meyer, *Nat. Commun.*, 2012, **3**.
31. X. Y. Huang and J. T. Groves, *Chem Rev*, 2018, **118**, 2491-2553.
32. X. Engelmann, I. Monte-Perez and K. Ray, *Angew. Chem. Int. Ed.*, 2016, **55**, 7632-7649.
33. M. M. Chen, P. S. Coelho and F. H. Arnold, *Adv. Synth. Catal.*, 2012, **354**, 964-968.
34. M. Ghosh, K. K. Singh, C. Panda, A. Weitz, M. P. Hendrich, T. J. Collins, B. B. Dhar and S. Sen Gupta, *J. Am. Chem. Soc.*, 2014, **136**, 9524-9527.
35. R. Singh, G. Ganguly, S. O. Malinkin, S. Demeshko, F. Meyer, E. Nordlander and T. K. Paine, *Inorg. Chem.*, 2019, **58**, 1862-1876.
36. M. Ghosh, S. Pattanayak, B. B. Dhar, K. K. Singh, C. Panda and S. Sen Gupta, *Inorg. Chem.*, 2017, **56**, 10852-10860.
37. K. P. Shing, B. Cao, Y. G. Liu, H. K. Lee, M. D. Li, D. L. Phillips, X. Y. Chang and C. M. Che, *J. Am. Chem. Soc.*, 2018, **140**, 7032-7042.
38. T. Kojima, K. I. Hayashi, S. Y. Iizuka, F. Tani, Y. Naruta, M. Kawano, Y. Ohashi, Y. Hirai, K. Ohkubold, Y. Matsuda and S. Fukuzumi, *Chem. Eur. J.*, 2007, **13**, 8212-8222.
39. I. Terao, S. Horii, J. Nakazawa, M. Okamura and S. Hikichi, *Dalton Trans.*, 2020, **49**, 6108-6118.
40. F. F. Pfaff, F. Heims, S. Kundu, S. Mebs and K. Ray, *Chem. Commun.*, 2012, **48**, 3730-3732.
41. T. Corona, F. F. Pfaff, F. Acuna-Pares, A. Draksharapu, C. J. Whiteoak, V. Martin-Diaconescu, J. Lloret-Fillol, W. R. Browne, K. Ray and A. Company, *Chem. Eur. J.*, 2015, **21**, 15029-15038.
42. Y. H. Qiu and J. F. Hartwig, *J. Am. Chem. Soc.*, 2020, **142**, 19239-19248.
43. W. Nam, I. Kim, Y. Kim and C. Kim, *Chem. Commun.*, 2001, 1262-1263.
44. W. Nam, J. Y. Ryu, I. Kim and C. Kim, *Tetrahedron Lett.*, 2002, **43**, 5487-5490.
45. O. V. Nesterova, M. N. Kopylovich and D. S. Nesterov, *RSC Adv.*, 2016, **6**, 93756-93767.
46. T. Nishiura, A. Takabatake, M. Okutsu, J. Nakazawa and S. Hikichi, *Dalton Trans.*, 2019, **48**, 2564-2568.
47. A. N. Bilyachenko, A. I. Yalymov, M. M. Levitsky, A. A. Korlyukov, M. A. Es'kova, J. Long, J. Larionova, Y. Guari, L. S. Shul'pina, N. S. Ikonnikov, A. L. Trigub, Y. V. Zubavichus, I. E. Golub, E. S. Shubina and G. B. Shul'pin, *Dalton Trans.*, 2016, **45**, 13663-13666.
48. A. Bell-Taylor, J. D. Gorden, E. E. Hardy and C. R. Goldsmith, *Inorg. Chim. Acta*, 2018, **482**, 206-212.
49. J. Nakazawa, A. Yata, T. Hori, T. D. P. Stack, Y. Naruta and S. Hikichi, *Chem. Lett.*, 2013, **42**, 1197-1199.
50. D. S. Nesterov, O. V. Nesterova, M. N. Kopylovich and A. J. L. Pombeiro, *Mol. Catal.*, 2018, **459**, 8-15.
51. O. V. Nesterova, K. V. Kasyanova, V. G. Makhankova, V. N. Kokozay, O. Y. Vassilyeva, B. W. Skelton, D. S. Nesterov and A. J. L. Pombeiro, *Appl. Catal. A*, 2018, **560**, 171-184.
52. O. V. Nesterova, K. V. Kasyanova, E. A. Buvaylo, O. Y. Vassilyeva, B. W. Skelton, D. S. Nesterov and A. J. L. Pombeiro, *Catalysts*, 2019, **9**, 15.
53. D. H. Wei, X. J. Zhu, J. L. Niu and M. P. Song, *ChemCatChem*, 2016, **8**, 1242-1263.
54. B. Wang, Y.-M. Lee, W.-Y. Tcho, S. Tussupbayev, S.-T. Kim, Y. Kim, M. S. Seo, K.-B. Cho, Y. Dede, B. C. Keegan, T. Ogura, S. H. Kim, T. Ohta, M.-H. Baik, K. Ray, J. Shearer and W. Nam, *Nat. Commun.*, 2017, **8**.
55. Y. M. Kwon, Y. Lee, G. E. Evenson, T. A. Jackson and D. Wang, *J. Am. Chem. Soc.*, 2020, **142**, 13435-13441.
56. G. Olivo, O. Lanzalunga and S. Di Stefano, *Adv. Synth. Catal.*, 2016, **358**, 843-863.
57. J. Serrano-Plana, W. N. Oloo, L. Acosta-Rueda, K. K. Meier, B. Verdejo, E. Garcia-Espana, M. G. Basallote, E. Munck, L. Que, A. Company and M. Costas, *J. Am. Chem. Soc.*, 2015, **137**, 15833-15842.
58. D. Font, M. Canta, M. Milan, O. Cusso, X. Ribas, R. J. M. K. Gebbink and M. Costas, *Angew. Chem. Int. Ed.*, 2016, **55**, 5776-5779.
59. B. Wang, Y. M. Lee, M. Clemancey, M. S. Seo, R. Sarangi, J. M. Latour and W. Nam, *J. Am. Chem. Soc.*, 2016, **138**, 2426-2436.
60. G. D. Roiban, R. Agudo and M. T. Reetz, *Angew. Chem. Int. Ed.*, 2014, **53**, 8659-8663.
61. R. Karande, L. Debor, D. Salamanca, F. Bogdahn, K. H. Engesser, K. Buehler and A. Schmid, *Biotechnol. Bioeng.*, 2016, **113**, 52-61.
62. A. Ilie, R. Agudo, G. D. Roiban and M. T. Reetz, *Tetrahedron*, 2015, **71**, 470-475.
63. G. B. Shul'pin, M. V. Kirillova, L. S. Shul'pina, A. J. L. Pombeiro, E. E. Karslyan and Y. N. Kozlov, *Catal. Commun.*, 2013, **31**, 32-36.
64. O. V. Nesterova and D. S. Nesterov, *Catalysts*, 2018, **8**, 602.
65. M. S. Seo, N. H. Kim, K. B. Cho, J. E. So, S. K. Park, M. Clemancey, R. Garcia-Serres, J. M. Latour, S. Shaik and W. Nam, *Chem. Sci.*, 2011, **2**, 1039-1045.
66. S. N. Dhuri, K. B. Cho, Y. M. Lee, S. Y. Shin, J. H. Kim, D. Mandal, S. Shaik and W. Nam, *J. Am. Chem. Soc.*, 2015, **137**, 8623-8632.
67. J. R. Bryant, T. Matsuo and J. M. Mayer, *Inorg. Chem.*, 2004, **43**, 1587-1592.

68. G. B. Shul'pin, D. S. Nesterov, L. S. Shul'pina and A. J. L. Pombeiro, *Inorg. Chim. Acta*, 2017, **455**, 666-676.
69. O. V. Nesterova, D. S. Nesterov, A. Krogul-Sobczak, M. F. C. Guedes da Silva and A. J. L. Pombeiro, *J. Mol. Catal. A*, 2017, **426**, 506-515.
70. G. S. Astakhov, A. N. Bilyachenko, A. A. Korlyukov, M. M. Levitsky, L. S. Shul'pina, X. Bantreil, F. Lamaty, A. V. Vologzhanina, E. S. Shubina, P. V. Dorovatovskii, D. S. Nesterov, A. J. L. Pombeiro and G. B. Shul'pin, *Inorg. Chem.*, 2018, **57**, 11524-11529.
71. O. V. Nesterova, D. S. Nesterov, B. Vranovicova, R. Boca and A. J. L. Pombeiro, *Dalton Trans.*, 2018, **47**, 10941-10952.
72. I. Gryca, K. Czerwinska, B. Machura, A. Chrobok, L. S. Shul'pina, M. L. Kuznetsov, D. S. Nesterov, Y. N. Kozlov, A. J. L. Pombeiro, I. A. Varyan and G. B. Shul'pin, *Inorg. Chem.*, 2018, **57**, 1824-1839.
73. K. L. Vikse, Z. Ahmadi and J. S. McIndoe, *Coord. Chem. Rev.*, 2014, **279**, 96-114.
74. M. Y. Hyun, S. H. Kim, Y. J. Song, H. G. Lee, Y. D. Jo, J. H. Kim, I. H. Hwang, J. Y. Noh, J. Kang and C. Kim, *J. Org. Chem.*, 2012, **77**, 7307-7312.
75. R. H. Crabtree, *J. Organomet. Chem.*, 2014, **751**, 174-180.
76. D. S. Nesterov, O. V. Nesterova, M. F. C. Guedes da Silva and A. J. L. Pombeiro, *Catal. Sci. Technol.*, 2015, **5**, 1801-1812.
77. G. B. Shul'pin, D. A. Loginov, L. S. Shul'pina, N. S. Ikonnikov, V. O. Idrisov, M. M. Vinogradov, S. N. Osipov, Y. V. Nelyubina and P. M. Tyubaeva, *Molecules*, 2016, **21**, 1593.
78. W. Nam, M. H. Lim, S. K. Moon and C. Kim, *J. Am. Chem. Soc.*, 2000, **122**, 10805-10809.
79. M. Martinho, F. Banse, J. F. Bartoli, T. A. Mattioli, P. Battioni, O. Horner, S. Bourcier and J. J. Girerd, *Inorg. Chem.*, 2005, **44**, 9592-9596.
80. S. Shaik, S. Cohen, S. P. de Visser, P. K. Sharma, D. Kumar, S. Kozuch, F. Ogliaro and D. Danovich, *Eur. J. Inorg. Chem.*, 2004, 207-226.
81. E. M. Simmons and J. F. Hartwig, *Angew. Chem. Int. Ed.*, 2012, **51**, 3066-3072.
82. G. B. Shul'pin, Y. N. Kozlov, G. V. Nizova, G. Suss-Frank, S. Stanislas, A. Kitaygorodskiy and V. S. Kulikova, *J. Chem. Soc. Perkin Trans. 2*, 2001, 1351-1371.
83. F. Gozzo, *J. Mol. Catal. A*, 2001, **171**, 1-22.
84. W. N. Oloo and L. Que, *Acc. Chem. Res.*, 2015, **48**, 2612-2621.
85. K. Chen and L. Que, *J. Am. Chem. Soc.*, 2001, **123**, 6327-6337.
86. J. Bernadou and B. Meunier, *J. Chem. Soc. Chem. Commun.*, 1998, 2167-2173.
87. K. A. Lee and W. Nam, *J. Am. Chem. Soc.*, 1997, **119**, 1916-1922.
88. A. R. Jeong, J. W. Shin, J. H. Jeong, K. H. Bok, C. Kim, D. Jeong, J. Cho, S. Hayami and K. S. Min, *Chem. Eur. J.*, 2017, **23**, 3023-3033.
89. C. Kim, H. Ahn, J. Bae, M. Kim, K. Bok, H. Jeong and S. Lee, *Chem. Eur. J.*, 2017, **23**, 11969-11976.
90. A. S. Novikov, M. L. Kuznetsov, B. G. M. Rocha, A. J. L. Pombeiro and G. B. Shul'pin, *Catal. Sci. Technol.*, 2016, **6**, 1343-1356.
91. M. L. Kuznetsov, B. G. M. Rocha, A. J. L. Pombeiro and G. B. Shul'pin, *ACS Catal.*, 2015, **5**, 3823-3835.
92. B. G. M. Rocha, M. L. Kuznetsov, Y. N. Kozlov, A. J. L. Pombeiro and G. B. Shul'pin, *Catal. Sci. Technol.*, 2015, **5**, 2174-2187.